

Erasmus Mundus SpaceMaster

Czech Technical University
Luleå University of Technology

Master Thesis

Design and simulation of satellite attitude stabilization control laws

Author:

Sharathkumaar Mohanasundaram

Supervisor:

doc.ing.Martin Hromcik,Ph.D

A thesis submitted in fulfilment of the requirements
for the degree of Master in Science

May 2017

Czech Technical University in Prague
Faculty of Electrical Engineering

Department of Control Engineering

DIPLOMA THESIS ASSIGNMENT

Student: **Sharathkumar Mohanasundaram**

Study programme: Cybernetics and Robotics
Specialisation: Systems and Control

Title of Diploma Thesis: **Design and simulation of satellite attitude stabilization control laws**

Guidelines:

The goal of this thesis project is to develop a set of advanced control design tools and simulation validation scenarios related to control of spacecraft, accompanied with a comprehensible documentation / manual. The delivered results shall be used in lectures and labs of the MSc level course "Flight Control Systems" / "Control Systems for Aircraft and Spacecraft" in future.

1. Develop realistic models of satellites, for the purpose of the thesis, in MATLAB / Simulink.
2. Develop realistic models of the actuators and sensors subsystems.
3. Design and validate by simulations attitude control laws with thrusters.
4. Design and validate control laws based on reaction wheel.
5. Design and validate spin stabilizing scenarios.
6. Design and validate attitude control with a gimballed momentum wheel.
7. Develop attitude control schemes during thrust maneuvers.
8. Develop control laws for translational motions.

Bibliography/Sources:


Arthur Bryson Jr., Control of Spacecraft and Aircraft, Princeton University Press, 1994. (chapters 1-8).

Diploma Thesis Supervisor: doc.Ing. Martin Hromčík, Ph.D.

Valid until the summer semester 2016/2017


prof. Ing. Michael Šebek, DrSc.
Head of Department




prof. Ing. Pavel Ripka, CSc.
Dean

Prague, February 17, 2017

Declaration of Authorship

I ,Sharathkumaar Mohanasundaram , hereby declare that this thesis titled, "**Design and simulation of satellite attitude stabilization control laws**" and the work presented in it are my own. I authored this thesis independently without prohibited help of third parties. Furthermore, I declare that all reference are marked as such. I confirm that:

This work was done wholly or mainly while in candidature for a master degree at Czech Technical University. Where any part of this thesis has previously been submitted for a degree or any other qualification at this University or any other institution, this has been clearly stated.

Where I have consulted the published work of others, this is always clearly attributed. Where I have quoted from the work of others, the source is always given. With the exception of such quotations, this thesis is entirely my own work. I have acknowledged all primary sources of help.

Where the thesis is based on work done by myself jointly with others, I have made clear exactly what was done by others and what I have contributed myself.

Signature: Sharathkumaar Mohanasundaram

Date:15.06.2017

Erasmus Mundus SpaceMaster

Czech Technical University
Luleå University of Technology

Abstract

Martin Hromcik
Department of Control Engineering

Master in Science

Design and simulation of satellite attitude stabilization control Laws

by Sharathkumar Mohanasundaram

In this thesis the problem of spacecraft attitude control is investigated. Individual spacecraft dynamics are modelled and controlled with thrusters, reaction wheel, Gimbaled momentum wheel and their coupling effects are analysed. Also controlling during thrust manoeuvres using gimbaled engines, control of translational motion and validating spin stabilization criterias. The equation of motions were derived and it is conveniently put into dimensionless forms and their corresponding transfer functions are obtained. Using the linear-quadratic performance index, favourable weighting factors are determined and the control law is determined. This overall thesis work will discuss basic satellite attitude stabilization concepts and its validations.

Acknowledgements

I would like to thank my family and friends who encouraged me and given me, the moral support to follow my dream and embark in this journey.

Content

List of figures

List of tables

Notations used

Abbreviations

1 Motivation	1
1.1. Spacecraft Attitude Determination	1
1.2. Attitude determination	1
2 Attitude Sensors	2
2.1 Optical sensors	2
2.2 Orbital Gyrocompassing	3
2.3 Gyro	4
2.4 Inertial Measurement Units	4
3. Attitude control with Thrusters	5
3.1 Fast attitude control vs slow Attitude control	5
3.2 Fast Attitude control using proportional Thrusters	5
3.3 Fast attitude control using On-Off thrusters	6
3.3.1 Bang-Off-Bang Control	7
4 Attitude control with reaction wheels	11
4.1 Introduction	11
4.2 Control concept with Reaction wheel and gravity desaturation	12
4.3 Equation of motion, Earth-pointing satellite	12
5 Spin stabilization	18
5.1 Introduction	18
5.2 Nutation	18
5.3 Nutation Damping	21
6 Attitude Control with a Gimballed Momentum Wheel	26
6.1. Introduction	26
6.2 Single-gimbal momentum wheel	27

6.3 Dual-gimbal	27
6.4 Control Concept	28
6.4.1 Equations of Motion of the Spacecraft	29
6.4.2 Equations of motion of Gimbaled momentum wheel with two gimbals	29
6.4.3 Equations of Roll/Yaw system	30
6.4.4 Passive Roll/Yaw stabilization	31
6.4.5 Active Roll/Yaw control	35
7 Attitude control during thrust maneuvers	38
7.1 Introduction	38
7.2 Attitude control during thrust maneuvers using a Gimbaled engine	38
8 Control of translational motion	45
8.1 Introduction	45
8.2 Translational motions in space	45
8.3 Translational Motions in Circular Orbit	46
8.3.1 Stabilization of In-Track/Radial Motions	49
Conclusion and further works	54
References	55
Appendix	56

List of figures

Figure 2.1 - Earth Sensor Diagram	2
Figure 2.2 - Analog Sun Sensor	2
Figure 2.3 - Star Sensor	3
Figure 2.4 Aerospace Euler angles (NASA standard)	4
Figure 3.1 .Three axis attitude control thrusters,wheels,and sensors	5
Figure 3.2 Attitude control system with proportional thrusters and attitude sensor	6
Figure 3.3 Output vs Input with dead zone and hysteresis (Schmitt trigger)	7
Figure 3.4 Block diagram of Schmitt trigger used with a liner switching function	7
Figure 3.5 Phase plane path; attitude control using deadband hysteresis (Schmitt trigger)	8
Figure 3.6 Attitude control of Satellite using Bang-off-Bang control	9
Figure 3.7 Attitude controlled output using bang-off-bang thrusters	10
Figure 4.1 DC motor as Reaction wheel	11
Figure 4.2 Locus of closed-loop poles vs A for slow roll/yaw control using roll and yaw reaction wheels and gravity desaturation	15
Figure 4.3 Response to an impulsive roll disturbance for slow roll/yaw control using roll and yaw reaction wheels and gravity desaturation	16
Figure 4.4 Response to an impulsive roll disturbance for slow roll/yaw control using roll and yaw reaction wheels and gravity desaturation	17
Figure 5.1 Disk-shaped and rod-shaped spin stabilized spacecraft	18
Figure 5.2 Spinning spacecraft with nutation damping wheel	21
Figure 5.3 Root locus vs damping constant D for disk-like spacecraft with nutation damping wheel	23
Figure 5.4. Response of disk-like spacecraft with nutation damping wheel to an impulsive roll disturbance torque	23
Figure 5.5 Root locus vs damping constant D for rod-like spacecraft with nutation damping wheel.	24

Figure 5.6. Response of rod-like spacecraft with nutation damping wheel to an impulsive roll disturbance torque	24
Figure 5.7 Instability of a spacecraft when spun about its minor axis	25
Figure 6.1. Single Gimbal Control Moment Gyroscope	27
Figure 6.2. Double Gimbal Control Moment Gyroscope with outer and inner servo system	27
Figure 6.3. Spacecraft with gimbale momentum wheel (GMW)	28
Figure 6.4 Viscous damper	32
Figure 6.5. Response of S/C with a GMW with passive control of GMW to impulsive roll and yaw disturbance torques with viscous damper between S/C and outer gimbal	34
Figure 6.6 Locus of closed-loop poles vs K for active control of S/C with a GMW	36
Figure 6.7 Response of S/C with active control of a GMW to impulsive roll and yaw disturbance torques.	37
Figure 7.1 Nozzle movement with respect to the centre line during flight	39
Figure 7.2 Spacecraft with a gimbale main engine for pitch motion control	39
Figure 7.3 Spacecraft with a gimbale main engine	40
Figure 7.4 Spacecraft with gimbale engine; locus of LQ regulator poles vs weighting factor A	43
Figure 7.5 Spacecraft with gimbale engine; response to initial angular velocity	44
Figure 8.1 Locally-Horizontal-Vertical (LHV) coordinates for position deviation from circular orbits	46
Figure 8.2 Modes of translational motion in circular orbit	48
Figure 8.3 Stabilization of in-track/radial motion using proportional tangential thrusters; locus of LQ regulator poles vs A/B with n=1	51
Figure 8.4 Response of controlled spacecraft to an initial in-track error $\delta x(0)/R = -.001$ with orbital rate n=1	51
Figure 8.5 Stabilization of in-track/radial motion using proportional tangential thrusters; locus of LQ regulator poles vs A/B with orbital rate ,n=2	52

Figure 8.6 Response of controlled spacecraft to an initial in-track error $\delta x(0)/R = -.001$ with orbital rate $n=2$ 53

List of Tables

Table 3.1.Comparision of reaction wheels, Single Gimbal Control Moment Gyroscope and Double gimbal control moment gyroscope	26
Table 7.1 Advantage and Disadvantages of using a Gimbaled engine	44

Notations used

ϕ = Roll angle

θ = Pitch angle

ψ = Yaw angle

ϕ_G = Inner gimbal Roll angle

θ_G = Inner gimbal pitch angle

ψ_G = Inner gimbal yaw angle

p = Angular velocity with respect to roll

q = Angular velocity with respect to pitch

r = Angular velocity with respect to yaw

h = Spin angular momentum

H = Total angular momentum

H_x = Roll total angular momentum

H_z = Pitch total angular momentum

n = Orbit rate

e_x = Armature voltage for roll

e_z = Armature voltage for yaw

Q_{dy} = External disturbance torque,

Q_{cx} = Roll control torque

Q_{cy} = Pitch control torque

Q_{cz} = Yaw control torque

Q_f = Wheel-bearing friction torque

I_y = Moment of inertia of satellite in pitch axis

I_x = Moment of inertia of satellite in roll axis

I_z = Moment of inertia of satellite in yaw axis

I_s = Moment of inertia about spin axis

I_T = Moment of inertia about transverse axis

I_w = Moment of inertia of damper wheel

ω_T = Transverse component of angular velocity

β =Phase angle

γ =Nutation angle,

Ω =Angular velocity of damper wheel relative to the spacecraft

ω_n =Nutation frequency

D =Damping constant

J = Moment of inertia of wheel plus motor

i =Armature current in DC motor

e =Armature voltage

R = Armature resistance

N = Torque per unit current \equiv back emf per unit angular velocity,

c = viscous friction coefficient

Abbreviations

SRCE - Symmetric Root Characteristic Equation

SRL - Symmetric Root Locus

ADCS- Attitude Determination and Control System

GMW-Gimbaleed Moment Wheel

LEO - Low earth orbit

CCD - Charged Coupled Device

IMU - Inertial Measurement Unit

GMW- Gimbaled Momentum Wheel

CMG - Control Moment Gyro

TVC - Thrust Vector Control

1 Motivation

Modern spacecraft have an attitude determination and control system (ADCS), one of the most challenging problems for control engineers is the modelling of the spacecraft. The attitude and orbit control subsystem (AOCS) provides attitude information and maintains the required spacecraft attitude during all phases of the mission, starting at spacecraft separation from the launch vehicle and throughout its operational lifetime. The subsystem consists of redundant microprocessor-based control electronics, sun and earth sensors, gyros, momentum wheels (MWs), a reaction wheel (RW), magnetic torquers, thrusters, and solar array and trim tab positioners.[1]

1.1. Spacecraft Attitude Determination

Unlike orbit problems most of the advances in attitude determination and control are recent, having happened mostly since the launch of Sputnik on 1954. This can be exemplified by the fact that the prediction of the orbital motion of celestial bodies was the initial motivation for much of Newton's work. So while much has been researched and discovered in orbit analysis, much of the body of knowledge is centuries old unlike attitude analysis. [2]

Spacecraft's attitude analysis can be divided into three main areas: determination, forecasting and control. In this thesis attitude determination and control has been discussed briefly.

Attitude determination is the process of analysing how often the actuators are used to perform the desired function.eg: pointing at sun .Attitude control is the process of positioning the satellite in a particular direction or spinning the spacecraft at a certain angular velocity around a specific axis to achieve the mission requirement.

1.2. Attitude determination

The attitude determination of a spacecraft is inherently dependent on its mission profile. A spacecraft that is launched into Low Earth Orbit (LEO) does not have the same attitude determination system that an exploratory mission to Mars has. The sensors used, their number, the algorithms and data processing hardware are all different.

The accuracy of the determined attitude depends on the sensors, on the attitude determination algorithms used and on the hardware capability available. In order to fully determine a spacecraft's attitude it is necessary to have at least 2 linearly independent vectors [2].

Using just one vector it is not enough as it is not possible to know whether the spacecraft is spinning around said reference vector or not. This means that a single reference vector does not contain information to determine the spacecraft's rotation around this reference vector. Therefore, another reference vector is necessary to unambiguously fix the spacecraft's attitude.

2 Attitude Sensors

There exist many types of sensors to determine spacecraft attitude. Each of these sensors determine either angle or angular velocity with respect to a reference frame. A magnetometer measures the angle between the spacecraft's vector orientation with respect to Earth's magnetic field vector.

2.1 Optical sensors

A Sun sensor measures the angle between the spacecraft's vector orientation with respect to the vector the points from the spacecraft to the Sun, similarly to Earth sensors, which measures the angle between the spacecraft's vector orientation with respect to the vector the points from the spacecraft to the Earth.

Simplified schematics of an Earth sensor and a Sun sensor can be seen in Figures 1 and 2 respectively [3].

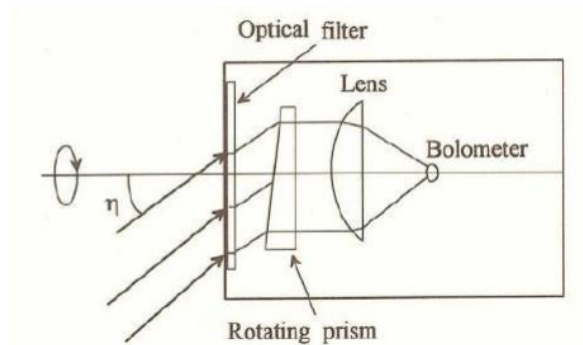


Figure 2.1 - Earth Sensor Diagram

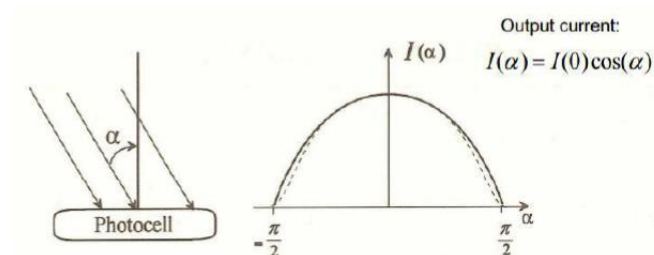


Figure 2.2 - Analog Sun Sensor

A star sensor measures angle with respect to the inertial frame of the universe. A simplified schematic of a star sensor can be seen in Figure 3. A CCD or other similar device captures the light coming from the stars in its field of view. This image is then amplified and compared with preloaded star charts in the memory of the sensor, when a match is found the sensor knows in which direction it is pointing.

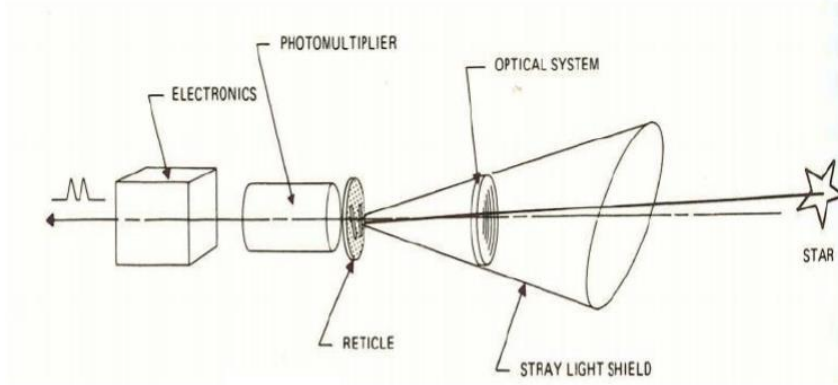


Figure 2.3 - Star Sensor

2.2 Orbital Gyrocompassing

Horizon sensors measure roll angle, ϕ and pitch angle, θ , but they obviously cannot measure yaw angle, ψ . However, if roll-rate and yaw-rate gyros are added (measuring p and r), then it is possible to estimate the yaw angle, using the kinematic roll/yaw coupling equations

$$\dot{\phi} = p + n\psi, \quad (2.1)$$

$$\dot{\psi} = r - n\phi \quad (2.2)$$

If the orbit rate, n is known, then ψ is observable from (1)

$$\psi = \frac{\dot{\phi} - p}{n} \quad (2.3)$$

Now, the horizon sensor measurement of ϕ is noisy, so it is not possible to differentiate the ϕ signal to find $\dot{\phi}$. A kinetic estimator, which uses (1) and (2), along with the measurements of ϕ , p and r (call them ϕ_m, p_m, r_m) as follows:

$$\dot{\hat{\phi}} = p_m + n\hat{\psi} + K_\phi(\phi_m - \hat{\phi}), \quad (2.4)$$

$$\dot{\hat{\psi}} = r_m - n\hat{\phi} + K_\psi(\phi_m - \hat{\phi}), \quad (2.5)$$

Where $(\hat{\phi}, \hat{\psi})$ are the estimators of (ϕ, ψ) . This estimator does not require the derivative of ϕ_m .

The estimate errors, $\tilde{\phi} = \hat{\phi} - \phi$ and $\tilde{\psi} = \hat{\psi} - \psi$, can be predicted by subtracting (1) and (2) from (4) and (5). If we consider (ϕ_m, p_m, r_m) are reasonably accurate, then

$$\dot{\hat{\phi}} = n\tilde{\psi} - K_{\phi}\tilde{\phi}, \quad (2.6)$$

$$\dot{\hat{\psi}} = -n\tilde{\phi} - K_{\psi}\tilde{\psi}. \quad (2.7)$$

The characteristic equation of (6)-(7) is

$$s(s+K_{\phi})+n(n+K_{\psi})=0. \quad (2.8)$$

If we wish the error decay eigen values to be $(-n,-n)$, the desired characteristic equation is :

$$(s + n)^2 \equiv s^2 + 2ns + n^2 = 0. \quad (2.9)$$

Comparing the coefficients of s in (7) and (8) gives the required gains:

$$K_{\phi} = 2n, \quad (2.10)$$

$$K_{\psi} = 0 \quad (2.11)$$

2.3 Gyro

The angular velocity of a spacecraft with respect to inertial space can be determined using three *rate gyros*. If the gyros are attached rigidly to the spacecraft, then the three measured angular velocities are in body-axis components. Current inertial platforms drift away from their initial positions at a rate of .01 to .001 deg/hr. Periodic sightings on celestial objects can be used to estimate the platform misalignment; in between sightings the platform provides a good estimate of current spacecraft attitude[4].

2.4 Inertial Measurement Units

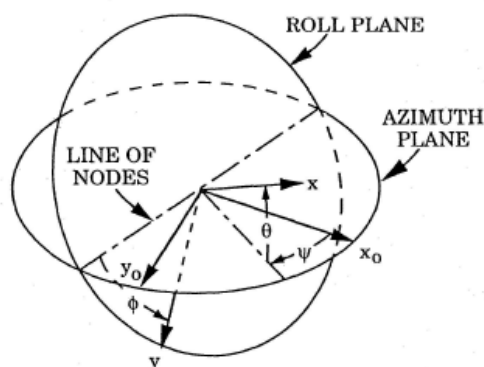


Figure 2.4 Aerospace Euler angles (NASA standard)

For this type of inertial measurement unit (IMU) a platform is mounted in gimbals relative to the spacecraft. Three gyros and three specific force sensors are mounted on the platform with their sensitive axes mutually orthogonal. Using the gyro signals, the gimbals are torqued to keep the angular velocity of the platform as close to zero as possible. The gimbal angles are then the Euler angles of the spacecraft with respect to inertial space (Figure 2.4) [4].

3 Attitude control with Thrusters

3.1 Fast attitude control vs slow Attitude control

If the desired attitude control bandwidth is large compared to orbit rate (n), then gravity or magnetic torques are small compared to the required control torques. Hence it can be used as a disturbance torques, using a free space model of satellite dynamics. This is call fast attitude control. On the other case if the control bandwidth is comparable to orbit rate, then the gravity or magnetic torques can be used with the reaction wheels to stabilize the satellite without use of thrusters it is called as Slow attitude control [4].

3.2 Fast Attitude control using proportional Thrusters

If the available control torques are large when compared to the external disturbance torques and wish to stabilize the spacecraft attitude with respect to inertial space, then the attitude motion about the three-principle axis may be treated separately as shown in the figure 3.1.

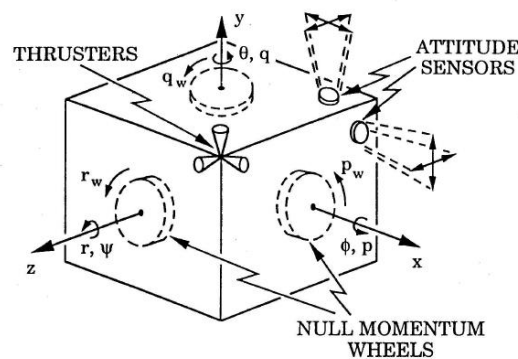


Figure 3.1 .Three axis attitude control thrusters,wheels,and sensors

A convenient inertial reference system in interplanetary space is the celestial sphere.

Proportional thrusters are not easy to achieve in practice. It is considered because it is simpler than control logic for the on-off thrusters.

If *both attitude and attitude rate are sensed* (e.g., using a sun sensor, a star sensor, and three rate gyros), then stabilization about each principal axis may be obtained by feeding back a linear combination of attitude deviation and attitude rate to the torquer. Here, the body y-axis, is considered.

$$Q_y = -D\dot{\theta} - K\theta, \quad (3.1)$$

where

$$I_y\ddot{\theta} = Q_y. \quad (3.2)$$

Clearly, for $D>0, K>0$, the motion is stabilized.

If only attitude is sensed, then the stabilization about each principle axis may be obtained by feeding back attitude deviation with lead compensation to the torque. Considering the body y-axis,

$$Q_y = -K(\theta - \xi), \quad (3.3)$$

$$\dot{\xi} + b\xi = (b - a)\theta. \quad (3.4)$$

In transfer function notation, (2)-(4) become

$$Q_y(s) = -K \frac{s+a}{s+b} \theta(s), \quad (3.5)$$

$$\theta(s) = \frac{1}{I_y s^2} Q_y(s). \quad (3.6)$$

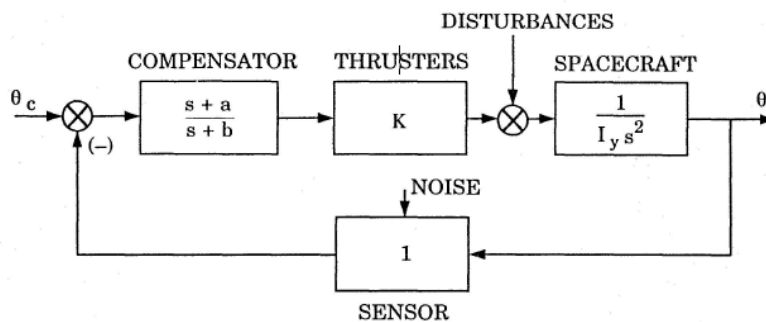


Figure 3.2 Attitude control system with proportional thrusters and attitude sensor

The characteristic equation of system (5) and (6), in Evans's form, is

$$-\frac{K}{I_y} = \frac{s^2(s+b)}{s+a}. \quad (3.7)$$

3.3 Fast attitude control using On-Off thrusters

With the complications with the proportional thrusters, on-off or bang-bang control have been developed. Valves can be operated to stay open as little as a few milliseconds and can be fired over million times reliably, but the valves has to open for a finite period of time. Hence, there

will be a discrete change in angular velocity with each actuation of the valve. To prevent opposing jets from firing each other, there must be a dead band in a system using on-off control. When the vehicle is in the deadband, no control is taken. When the error signal exceeds the deadband, then the gas valves are modulated. [4]

3.3.1 Bang-Off-Bang Control

To make effective use of a dead-zone we also use *hysteresis*; dead zone and hysteresis are combined in a scheme called a Schmitt trigger, shown in Figure 3.3. It is simple to use the Schmitt trigger with a *linear switching function* as shown in Figure 3.4.

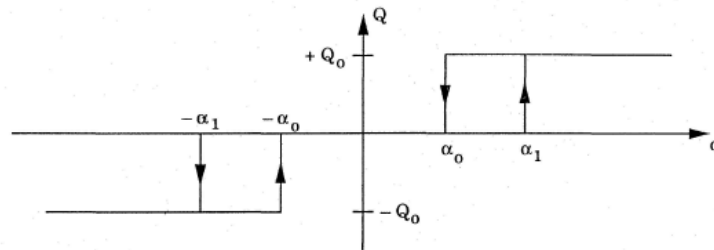


Figure 3.3 Output vs Input with dead zone and hysteresis (Schmitt trigger)

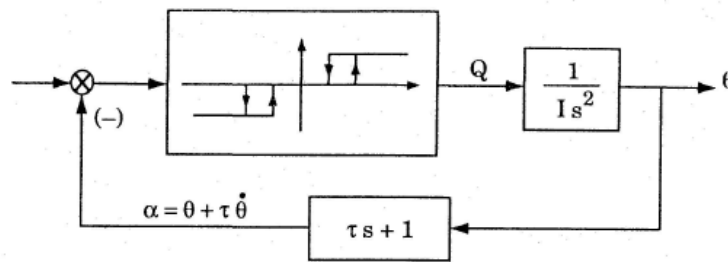


Figure 3.4 Block diagram of Schmitt trigger used with a linear switching function

This control system cannot bring θ and $\dot{\theta}$ to zero, but at least it can bring them to acceptably small values, ending with a low-frequency limit cycle, which does not use as much fuel as the bang-bang scheme. It is straightforward to show that the limit cycle period and amplitude are given by (figure 3.5)

$$\text{Period} = 4\tau \left(\frac{\alpha_1 - \alpha_0}{\alpha_1 - \alpha_0} + \frac{\alpha_1 - \alpha_0}{2N\tau^2} \right), N \triangleq \frac{Q_0}{I}, \quad (3.8)$$

$$\text{Amplitude} = \frac{1}{2}(\alpha_1 + \alpha_0) + \frac{1}{8} \frac{(\alpha_1 - \alpha_0)^2}{N\tau^2}. \quad (3.9)$$

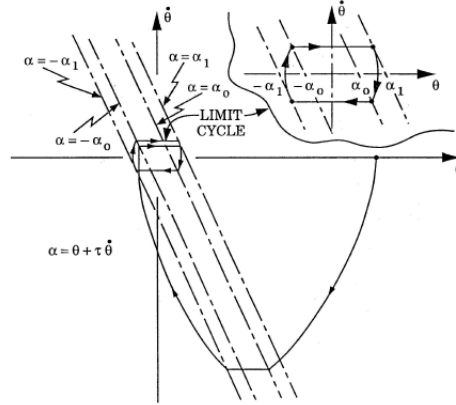


Figure 3.5 Phase plane path; attitude control using deadband hysteresis (Schmitt trigger)

For the fast attitude control, motion about each principle axis is nearly decoupled from motion about the other axes. Considering about the pitch (y) axis, and let q_w =angular velocity of the wheel with respect to inertial space. The satellite with reaction wheel's ,equations of motion are

$$I_y \dot{q} = Ni + Q_f + Q_{dy}, \quad (3.9)$$

$$\dot{\theta} = q, \quad (3.10)$$

$$Jq_w = -Ni - Q_f, \quad (3.11)$$

$$Ri = e - N(q - q_w), \quad (3.12)$$

$$Q_f = -c(q - q_w) \quad (3.13)$$

where

Q_{dy} =external disturbance torque,

Q_f =wheel-bearing friction torque,

I_y = moment of inertia of satellite,

J =Moment of inertia of wheel plus motor,

i =armature current in DC motor,

e =armature voltage,

R =armature resistance,

N = torque per unit current \equiv back emf per unit angular velocity,

c =viscous friction coefficient.

For the modelling, the following parameters are considered.

$$R=100 \text{ ohms}$$

$$N=0.1$$

$$c = -0.879 \cdot 10^{-4} \text{ Nms}$$

$$J=4.95 \cdot 10^{-3} \text{ Kgm}^2$$

$$I=0.1 \cdot 10^{-3} \text{ Kgm}^2$$

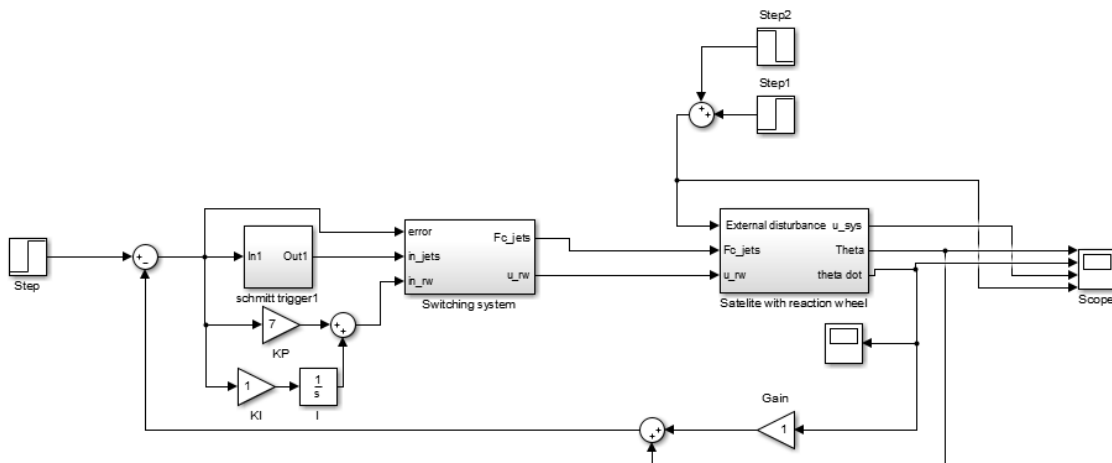


Figure 3.6 Attitude control of Satellite using Bang-off-Bang control

Figure 3.6 shows the attitude control of satellite using bang-off –bang control thrusters as actuator. The system is modelled based on the block diagram, figure 3.4. PI controller is designed to regulate the changes occurring due to external disturbances. Initially system will be in zero initial condition. If any external disturbance enters the system it is sensed by the feedback controller, which sends impulse to the jets to bring, back the system to the stable normal position.

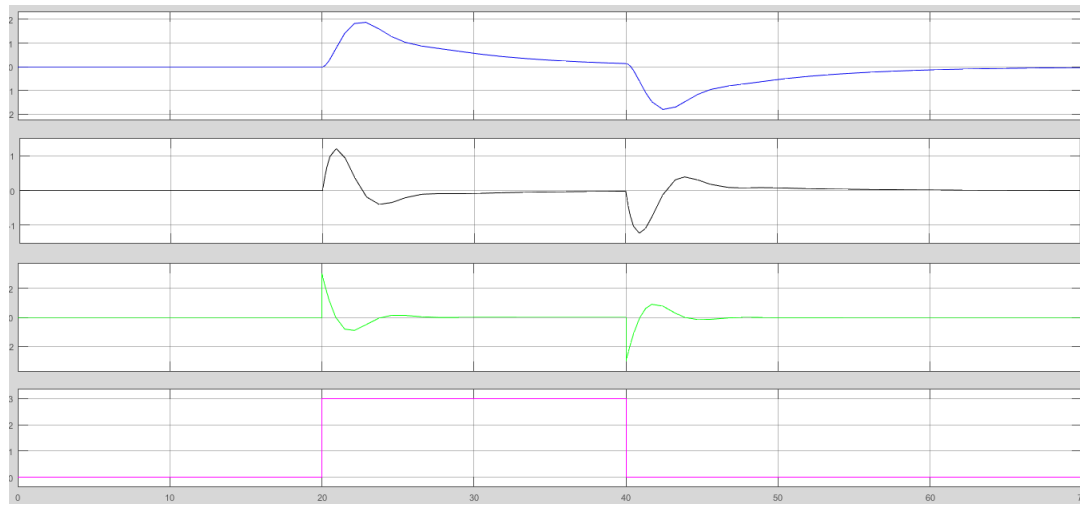


Figure 3.7 Attitude controlled output using bang-off-bang thrusters

Figure 3.8 shows the attitude-controlled output of satellite with reaction wheel using bang-off-bang control. The first block with blue line is the θ . The second block with black line is $\dot{\theta}$. And the yellow line is the disturbance. External disturbance is introduced into the system between 20 to 40 seconds. Both θ and $\dot{\theta}$ spikes when the disturbance is given and because of the control action of the controller both θ and $\dot{\theta}$ returns to very low values approximately equal to zero, which shows that the attitude is controlled satisfactorily for the applied disturbance.

4 Attitude control with reaction wheels

4.1 Introduction

Pointing accuracy of the on-off thrusters is limited to 0.1 to 1.0 degrees. In case of the pointing a telescope more accuracy is needed. In case of such requirements, reaction wheels are used. The main concept in case of using reaction wheels is to put the unwanted spacecraft angular momentum caused by the external disturbances into the wheels. This is possible with the proportional electromagnetic torquers such as DC motors. Hence, a very precise control of satellite attitude is possible. Moreover using thrusters may utilize spacecraft's fuel to an extent. So implementing reaction wheel may help to reduce the fuel consumption.

The use of a reaction wheel as an actuator in satellite control has gained popularity lately [5-7]. Some advantages of this type of actuator configuration over others are shown in [6]. A reaction wheel is a device that applies torque to satellite at the control command resulting in changed angular momentum (or angular velocity) of the satellite. However, the presence of disturbances and uncertainties in reaction wheel itself can significantly deteriorate control performance and must be compensated for in the control design [8].

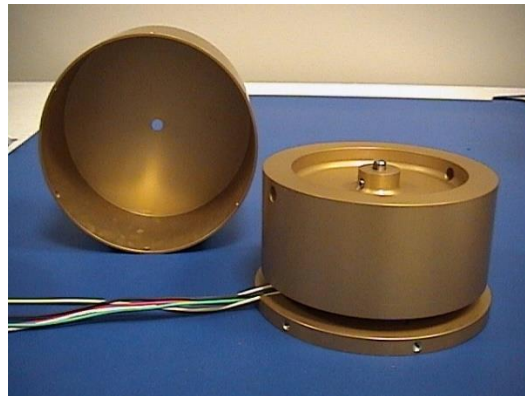


Figure 4.1 DC motor as Reaction wheel

A reaction wheel (RW) is a type of flywheel used primarily by spacecraft for attitude control without using fuel for rockets or other reaction devices. They are particularly useful when the spacecraft must be rotated by very small amounts, such as keeping a telescope pointed at a star. They may also reduce the mass fraction needed for fuel. This is accomplished by equipping the spacecraft with an electric motor attached to a flywheel. When its rotation speed is changed, it causes the spacecraft to begin to counter-rotate proportionately through conservation of angular momentum. Reaction wheels can rotate a spacecraft only around its centre of mass. They are not capable of moving the spacecraft from one place to another. Reaction wheels work around a nominal zero rotation speed. However, external

torques on the spacecraft may require a gradual build-up of reaction wheel rotation speed to maintain the spacecraft in a fixed orientation [9].

4.2 Control concept with Reaction wheel and gravity desaturation

If the wheel angular velocity becomes too large, thrusters are fired to desaturate the wheels. In low earth orbit, there are external torques available for desaturation, namely gravity and magnetic torques. Magnetic torques are produced by electric currents on the spacecraft interacting with the earth's magnetic field. These are both very small torques, and desaturation time constants are on the order of an orbit period. To use gravity torque in this manner, the spacecraft pitch angle must be perturbed slightly from the desired equilibrium attitude. Magnetic torques have the advantage that the pitch angle can be held at zero and the current coils must be oriented properly with respect to the earth's magnetic field, which adds some complication [4].

For fast control, small attitude perturbations about each axis are uncoupled from each other. For slow control in circular orbit, the pitch motion is decoupled, but the roll and yaw motions are coupled; control of roll/yaw is discussed in this part.

Roll and yaw motions of an earth-pointing spacecraft are coupled in orbit. While it is possible to stabilize both, roll and yaw with only a roll reaction wheel. We consider the case with reaction wheels on both the roll axis and the yaw axis; the roll gravitational torque can be used to desaturate both roll and yaw reaction wheels.

4.3 Equation of motion ,Earth-pointing satellite

Considering the spacecraft body axes are the principle axis, the moment of momentum of the spacecraft is

$$\vec{H} = I_x p \hat{i} + I_y q \hat{j} + I_z r \hat{k} \quad (4.1)$$

The equations of motion for small perturbations from locally horizontal axes decouple into two sets, one for pitch and one for roll/yaw.

Roll/yaw set is :

$$I_x \dot{p} = -n(I_y - I_z)r - 3n^2(I_y - I_z)\phi + N_x i_x + Q_{fx} + Q_{dx} \quad (4.2)$$

$$I_z \dot{r} = -n(I_y - I_x)p + N_z i_z + Q_{fz} + Q_{dz} \quad (4.3)$$

$$\dot{\phi} = n\psi + p, \quad (4.4)$$

$$\dot{\psi} = -n\phi + R, \quad (4.5)$$

Where $n \triangleq \sqrt{g/R}$ = orbital angular velocity, (Q_x, Q_z) are the external torques and (N_x, N_z) are the torque per unit current. The gyroscopic coupling terms, $n(I_y - I_z)r$ in (4.3) and $n(I_y - I_z)p$ in (4.4), arise from the rotation of the locally horizontal axes at orbit rate n .

$$J_x \dot{p}_w = -N_x i_x - Q_{fx}, \quad (4.6)$$

$$J_z \dot{r}_w = -N_z i_z - Q_{fz}, \quad (4.7)$$

$$R_x i_x = e_x + N_x (p_w - p), \quad (4.8)$$

$$R_z i_z = e_z + N_z (r_w - r), \quad (4.9)$$

$$Q_{fx} = -c_x (p - p_w), \quad (4.10)$$

$$Q_{fz} = -c_z (p - r_w). \quad (4.11)$$

Where (e_x, e_z) are the armature voltage of the roll, yaw reaction wheel motors, and the control variables here

$H_x = I_x p + J_x p_w$ = total roll angular momentum, and $H_z = I_z r + J_z r_w$ = total yaw angular momentum, as state variables in place of p_w and r_w , which are angular velocities of the roll and yaw reaction wheels, so that

$$p_w = \frac{H_x - I_x p}{J_x} \quad (4.12)$$

$$r_w = \frac{H_z - I_z r}{J_z}, \quad (4.13)$$

Adding the \dot{p} and \dot{p}_w equations and the \dot{r} and \dot{r}_w equations eliminates the internal torques $N_x i_x, N_z i_z, Q_{fx}, Q_{fz}$, giving

$$\dot{H}_x = -n(I_y - I_z)r - 3n^2(I_y - I_z)\phi + Q_{dx}, \quad (4.14)$$

$$\dot{H}_z = -n(I_y - I_x)r + Q_{dz}. \quad (4.15)$$

Substituting (8)-(13) into (2)-(3) gives

$$\dot{p} = -ar - 3a\phi - \sigma_x p + \frac{\sigma_x(1-\varepsilon_x)H_x}{I_x} + b_x e_x + \frac{Q_{dx}}{I_x} \quad (4.16)$$

$$\dot{r} = bp - \sigma_z r + \frac{\sigma_z(1-\varepsilon_z)H_z}{I_z} + b_z e_z + \frac{Q_{dz}}{I_z} \quad (4.17)$$

where times is in units of $1/n$, (p, r) in n , (H_x, H_z) in $(I_x n, I_z n)$, (e_x, e_z) in $(\frac{I_x n^2 R_x}{N_x}, \frac{I_z n^2 R_z}{N_z})$, (Q_{dx}, Q_{dz}) in $(I_x n^2, I_z n^2)$ and

$$\sigma_x = (c_x + N_x^2/R_x)(\frac{1}{J_x} + \frac{1}{I_x})/n^2,$$

$$\sigma_z = (c_z + N_z^2/R_z)(\frac{1}{J_z} + \frac{1}{I_z})/n^2,$$

The motor time constants $1/\sigma_x$ and $1/\sigma_y$ will, in general, be much smaller than the orbit period $2\pi/n$, so two very different time scales to consider. The shorter one corresponds to the time to transfer angular momentum to the reaction wheels; the longer one to the desaturation of the wheels and the attenuation of the roll and yaw angles to zero.

The equations of motion are given by

$$\dot{\phi} = [p] + n[\psi], \quad (4.18)$$

$$\dot{p} = -3an^2[\phi] - [p] + \frac{I_x}{I_x + J_x}[H_x] - an[r] + [e_x], \quad (4.19)$$

$$\dot{H}_x = -3an^2[\phi] - an[r], \quad (4.20)$$

$$\dot{\psi} = -n[\phi] + [H_z], \quad (4.21)$$

$$\dot{r} = bn[p] + [r] + \frac{I_z}{I_z + J_z}[H_z] + [e_z], \quad (4.22)$$

$$\dot{H}_z = bn[p]. \quad (4.23)$$

where

$$\varepsilon_x = J_x/I_x,$$

$$\varepsilon_z = J_z/I_z,$$

$$a = (I_y - I_z)/I_x,$$

$$b = (I_y - I_x)/I_z.$$

then the state space representation of above equations are given by

$$\begin{bmatrix} \dot{\phi} \\ \dot{p} \\ \dot{H}_x \\ \dot{\psi} \\ \dot{r} \\ \dot{H}_z \end{bmatrix} \cong \begin{bmatrix} 0 & 1 & 0 & n & 0 & 0 \\ -3an^2 & -1 & \frac{1}{1+\epsilon_x} & 0 & -an & 0 \\ -3an^2 & 0 & 0 & 0 & -an & 0 \\ -n & 0 & 0 & 0 & 1 & 0 \\ 0 & bn & 0 & 0 & -1 & \frac{1}{1+\epsilon_z} \\ 0 & bn & 0 & 0 & 0 & 0 \end{bmatrix} \begin{bmatrix} \phi \\ p \\ H_x \\ \psi \\ r \\ H_z \end{bmatrix} + \begin{bmatrix} 0 & 0 \\ 1 & 0 \\ 0 & 0 \\ 0 & 0 \\ 0 & 1 \\ 0 & 0 \end{bmatrix} \begin{bmatrix} e_x \\ e_z \end{bmatrix}$$

Considering the *oblate, axially symmetric S/C* where $a = b = 1/2$, with its symmetry axis cross-track with $\epsilon_x = \epsilon_y = 0.025$. This uncontrolled *S/C* has two undamped oscillatory modes with frequencies $1.523n$ and $0.657n$. Since they involve primarily roll and yaw motions respectively, it can be called as the roll and yaw modes.

Considering the performance index

$$J = \int_0^{\infty} [A(\phi^2 + \psi^2) + ex^2 + ez^2] dt.$$

For $n = \sigma/50$, the locus of closed-loop poles vs. A is shown in Figure 4.2. The reaction wheel poles are changed only slightly for the range of A used in the plot, while the roll and yaw mode poles are changed significantly.

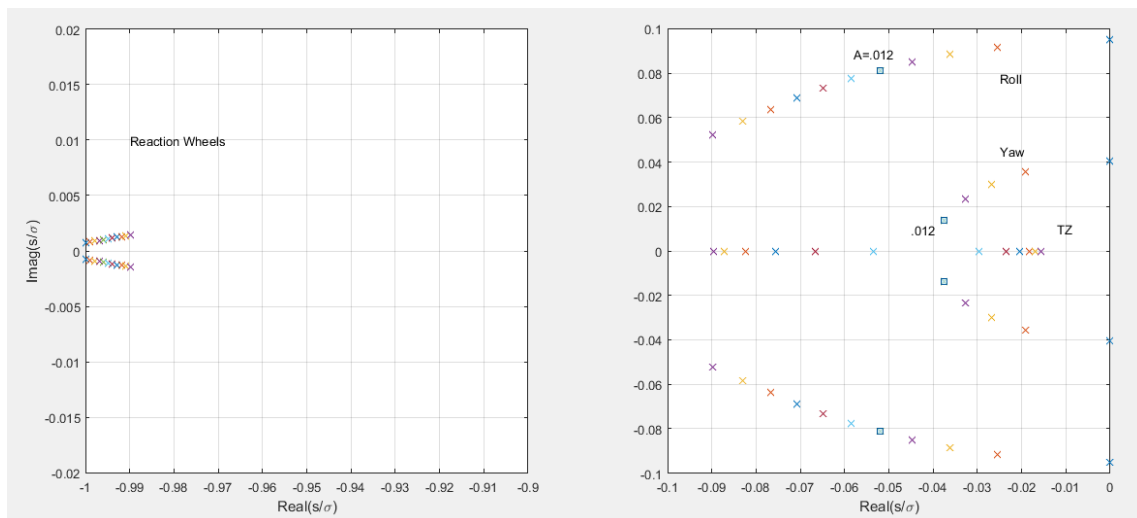


Figure 4.2 Locus of closed-loop poles vs A for slow roll/yaw control using roll and yaw reaction wheels and gravity desaturation

Choosing $A = .012$, for which the corresponding closed loop poles are

$$s = -0.037 \pm 0.0139j, -0.052 \pm 0.0813j$$

and its state feedback control law

$$\begin{bmatrix} e_x \\ e_z \end{bmatrix} = \begin{bmatrix} -0.1089 & -0.1036 & 0 & -0.006 & 0 & -0.0009 \\ 0.0065 & 0 & .0009 & -0.109 & -0.104 & 0 \end{bmatrix} \begin{bmatrix} \phi \\ p \\ H_x \\ \psi \\ r \\ H_z \end{bmatrix}$$

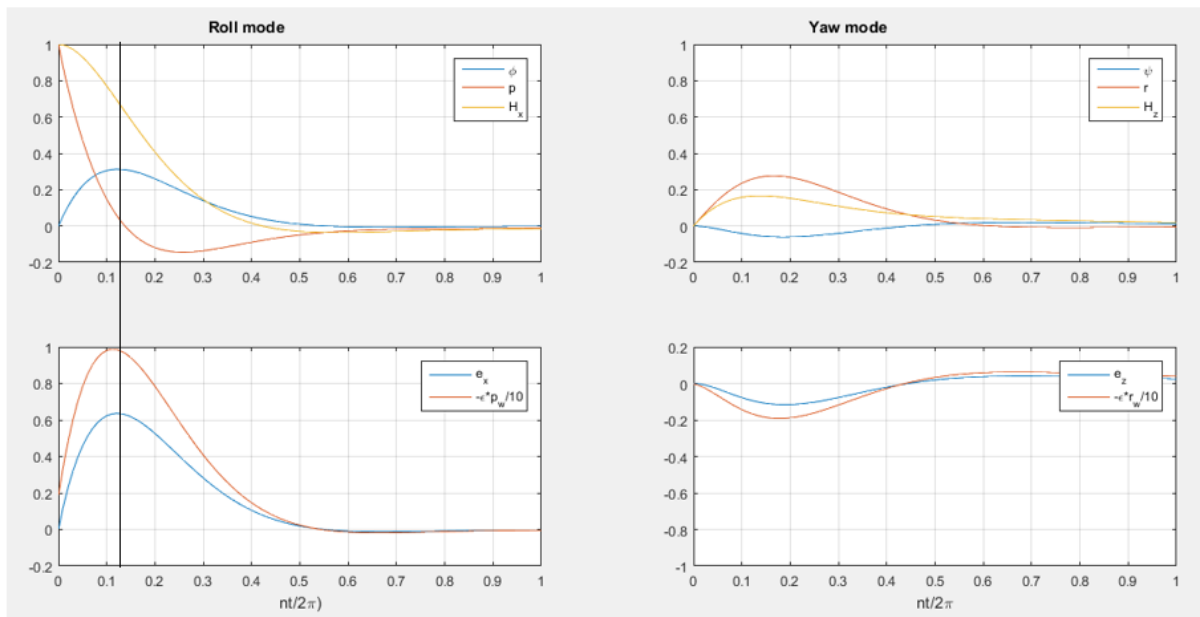


Figure 4.3 Response to an impulsive roll disturbance for slow roll/yaw control using roll and yaw reaction wheels and gravity desaturation

Figure 4.3 shows the response of the closed-loop system to a roll disturbance torque of magnitude $I_x n$. The roll angular momentum is transferred to the roll reaction wheel by $nt/2\pi = 0.13$ where ϕ reaches its peak value; then follows the desaturation period, which is essentially completed in one orbit ($nt = 2\pi$). The angular velocity with respect to roll (p) also decreases. Also, the yaw coupling is small but non-negligible.

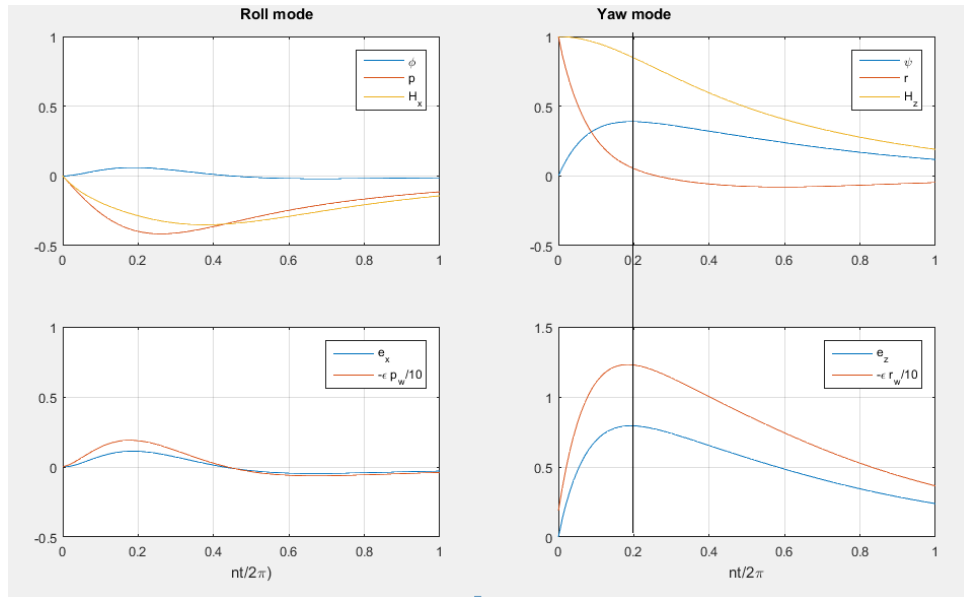


Figure 4.4 Response to an impulsive roll disturbance for slow roll/yaw control using roll and yaw reaction wheels and gravity desaturation

Figure 4.4 shows the response of the closed-loop system to a yaw disturbance torque of magnitude $I_z n$. The yaw angular momentum is transferred to the yaw reaction wheel by $\frac{nt}{2\pi} = 0.2$ where ψ reaches its peak value; then follows the desaturation period, which is completed approximately in 1.5 orbits. The roll coupling is large, since the gravity torque acts only in roll, not in yaw.

The only disadvantage of the reaction wheel is that it can become saturated, in which case momentum dumping would be required. However, this can be compensated by designing a wheel with a larger inertia than necessary [10].

5 Spin stabilization

5.1 Introduction

Imparting spin to a body is a simple and a passive method of stabilizing its attitude. A rigid body with its angular velocity parallel to its major axis which is the principal axis passing through the centre of mass, having maximum moment of inertia will maintain this axis in a fixed direction with respect to inertial space in the absence of external torques. Spin stabilization is mainly used to position the satellites in orbits.

5.2 Nutation

If the angular velocity of a rigid body is *not* parallel to its major or minor axis, the body is considered to be nutating. The angular momentum vector, \vec{H} , is fixed with respect to inertial space if there are no external torques, but the angular velocity vector, $\vec{\omega}$, rotates around the angular momentum vector.

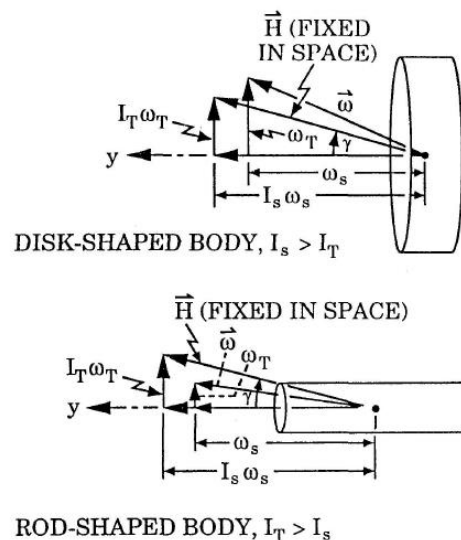


Figure 5.1 Disk-shaped and rod-shaped spin stabilized spacecraft

For *axially symmetric bodies*, \vec{H} , $\vec{\omega}$, and the axis of symmetry are co-planar as in Figure. 5.1. The symmetry axis (hence also the $\vec{\omega}$, vector) rotates about the fixed \vec{H} vector at a constant rate called the *nutation frequency*. If the axis of geometric symmetry is not a principal axis, the body is said to be *dynamically unbalanced*; even when nutation is absent, such a body will appear to *vibrate*. [4]

Let the y-axis be the axis of symmetry which is the nominal spin axis. It is considered because the spin axis of most satellites is perpendicular to the orbit plane and the coordinates are taken in this as the y-axis (pitch axis). Let I_s =moment of inertia about the spin axis and I_T = moment of inertia about the two transverse axes, x and z . Nonspinning body axes are considered as the coordinate axes, that is, axes that roll ($p \neq 0$) and yaw ($r \neq 0$) with the body but do not spin (pitch) with it; the components of the angular velocity of these coordinate axes with respect to inertial space resolved onto themselves is given by

$$\vec{\omega}_c = [p \ 0 \ r]^T \quad (5.1)$$

The components of angular momentum, resolved onto these axes, are

$$\vec{H} = [I_T p \ I_s \omega_s \ I_T r]^T, \quad (5.2)$$

Where ω_s =spin angular velocity .consequently, Euler's law,

$$\vec{H}^I \equiv \vec{H}^c + \vec{\omega}_c \times \vec{H} = 0, \quad (5.3)$$

In terms of these components is given by

$$I_T \dot{p} - (I_s \omega_s) r = 0, \quad (5.4)$$

$$I_s \dot{\omega}_s = 0, \quad (5.5)$$

$$I_T \dot{r} - (I_s \omega_s) p = 0, \quad (5.6)$$

(5) Implies that

$$\omega_s = \text{constant}, \quad (5.7)$$

So that (4) and (6) may be written as

$$\begin{aligned} \dot{p} - \omega_n r &= 0, \\ \dot{r} - \omega_n p &= 0, \end{aligned} \quad (5.8)$$

where

$$\omega_n \triangleq \frac{I_s}{I_T} \omega_s. \quad (5.9)$$

is the nutation frequency as observed in these non-spinning co-ordinates. Hence, it is also the nutation frequency as seen by an observer at rest in an inertial reference frame. The general solution to (8) is

$$\begin{aligned} p &= \omega_T \sin(\omega_n t + \beta), \\ r &= \omega_T \cos(\omega_n t + \beta), \end{aligned} \quad (5.10)$$

where

$$\begin{aligned} \omega_T &= \text{transverse component of angular velocity} \\ \beta &= \text{phase angle} \end{aligned}$$

For a solid circular cylinder of radius r and length l ,

$$\frac{I_S}{I_T} = \frac{r^2/2}{\frac{r^2}{4} + l^2/12} = \frac{2}{1 + l^2/3r^2} \quad (5.11)$$

Thus, for a *disk-shaped body* ($C < \sqrt{3}r$), spin is about the *major axis*, and it follows from (9) that $\omega_s < \omega_n < 2\omega_s$, (5.12)

that is, the nutation frequency is higher than the spin rate. For a *rod-shaped body* ($C > \sqrt{3}r$), spin is about the minor axis, and

$$0 < \omega_n < \omega_s, \quad (5.13)$$

that is, the nutation frequency is lower than the spin rate. Consequently, to an observer in spinning body axes, the nutation of a rod-shaped body appears to be in the opposite direction to the spin.

For small roll and yaw Euler angles (ϕ, ψ), of the non-spinning body axes,

$$\begin{aligned} \dot{\phi} &\cong p, \\ \dot{\psi} &\cong r \end{aligned} \quad (5.14)$$

Substituting (10) into (14) and integrating gives

$$\begin{aligned} \phi &\cong -\frac{\omega_T}{\omega_n} \cos(\omega_n t + \beta), \\ \psi &\cong \frac{\omega_T}{\omega_n} \sin(\omega_n t + \beta), \end{aligned} \quad (5.15)$$

So, the *nutation angle*, γ , is approximately

$$\gamma \cong \frac{\omega_T}{\omega_n} \equiv \frac{I_T \omega_T}{I_S \omega_s},$$

which checks Figure 5.2 since the nutation angle is the angle between \vec{H} and they-axis.

5.3 Nutation Damping

If an external arrangement on a spinning spacecraft is arranged such that relative motion occurs between the part and the spacecraft when nutation is present in which the angular velocity not parallel to angular momentum and no relative motion occurs when nutation is absent, the nutation will be damped out if the relative motion dissipates energy, provided that the spin axis is the principal axis with *maximum moment of inertia*. [4]

A damped wheel, pendulum, or spring mass can be used, or a viscous fluid in an appropriately shaped container.

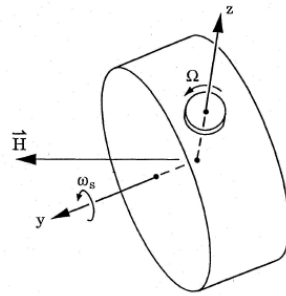


Figure 5.2 Spinning spacecraft with nutation damping wheel

Considering a damped wheel, where the wheel axis is perpendicular to the spin axis as shown in Figure 5.2. In body-fixed (spinning) coordinates, the angular velocity of the spacecraft is (p, ω_s, r) and the angular momentum is

$$\vec{H} = [I_T p \quad I_S \omega_s \quad I_T r + I_W \Omega],$$

where (I_T, I_S, I_W) are the principal moments of inertia of the spacecraft including the damper wheel at $\Omega = 0$, $I_W =$ moment of inertia of damper wheel about its free axis (the spacecraft z-axis), and $\Omega =$ angular velocity of damper wheel relative to the spacecraft.

Spacecraft angular momentum is changed only by external disturbance torques so

$$\vec{H}^B + \vec{\omega}_B \times \vec{H} = \vec{Q}_d \text{ gives}$$

$$I_T \dot{p} - (I_S - I_T) \omega_s r + I_W \omega_s \Omega = Q_{dx}, \quad (5.16)$$

$$I_S \dot{\omega}_s - I_W \Omega p = Q_{dy}, \quad (5.17)$$

$$I_T \dot{r} - (I_S - I_T) \omega_s r + I_W \dot{\omega} = Q_{dz}. \quad (5.18)$$

The components of damper wheel angular momentum in body-fixed axes are

$$[I_{WT} p, I_{WT} \omega_s, I_W (r + \Omega)],$$

and the wheel has a damping torque $-D\Omega$. Thus, about the z-axis,

$$I_W (\dot{r} + \dot{\Omega}) = -D\Omega. \quad (5.19)$$

The term $I_W \Omega p$ in (17) is usually negligible so that $\omega_s \approx \text{constant}$ if $Q_{dy} \approx 0$. Thus, the system equations may be written as

$$\begin{bmatrix} 1 & 0 & 0 \\ 0 & 1 & \epsilon \\ 0 & 1 & 1 \end{bmatrix} \begin{bmatrix} \dot{p} \\ \dot{r} \\ \dot{\Omega} \end{bmatrix} = \begin{bmatrix} 0 & \lambda - 1 & -\epsilon \\ -(\lambda - 1) & 0 & 0 \\ 0 & 0 & -D \end{bmatrix} \begin{bmatrix} p \\ r \\ \Omega \end{bmatrix} + \begin{bmatrix} Q_{dx} \\ Q_{dy} \\ 0 \end{bmatrix}, \quad (5.20)$$

where time is in units of $1/\omega_s$, (p, r, Ω) are in units of ω_s , D is in units of $I_W \omega_s$, and

$$\epsilon \triangleq \frac{I_W}{I_T},$$

$$\lambda \triangleq \frac{I_S}{I_T}.$$

Note $(\lambda - 1)\omega_s$ = the nutation frequency as viewed in the spinning body axes.

The characteristic equation of (20) is written in Evans's form as

$$-\frac{D}{1-\epsilon} = \frac{s(s^2+z^2)}{s^2+(\lambda-1)^2}, \quad (5.21)$$

where

$$z^2 \triangleq \frac{(\lambda-1)(\lambda-1+\epsilon)}{1-\epsilon}.$$

For disc-shaped spacecraft, $I_S > I_T$, which implies $(\lambda-1)^2 < z^2$ that is, the zero of the root locus is between the rigid-body pole and the nutation pole ; a root locus versus D (see Fig. 5.3) shows that the spacecraft is stabilized, that is, the nutation is damped.

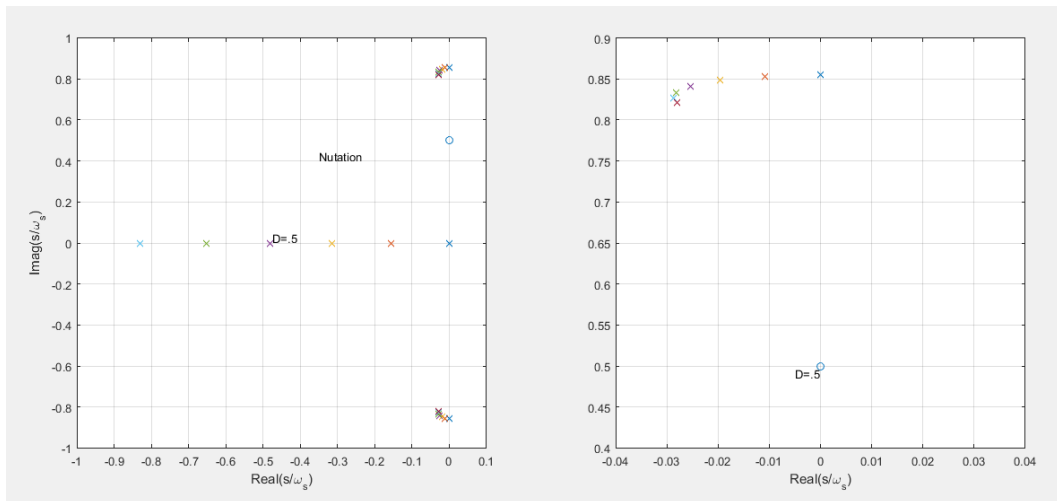


Figure 5.3 Root locus vs damping constant D for disk-like spacecraft with nutation damping wheel

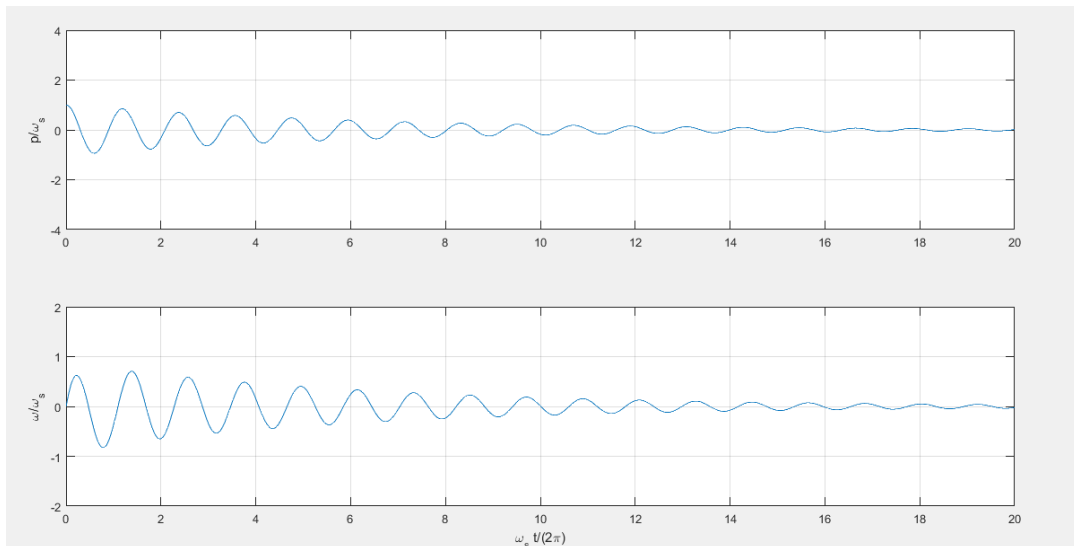


Figure 5.4. Response of disk-like spacecraft with nutation damping wheel to an impulsive roll disturbance torque

Fig. 5.4 shows the response of the system to an impulsive roll disturbance torque for the case $\lambda=1.8$, $\epsilon=.06$, $D = .5$. In which the angular velocity of the damper wheel, ω gets stable after certain period of time, which shows that the damper wheel becomes stable.

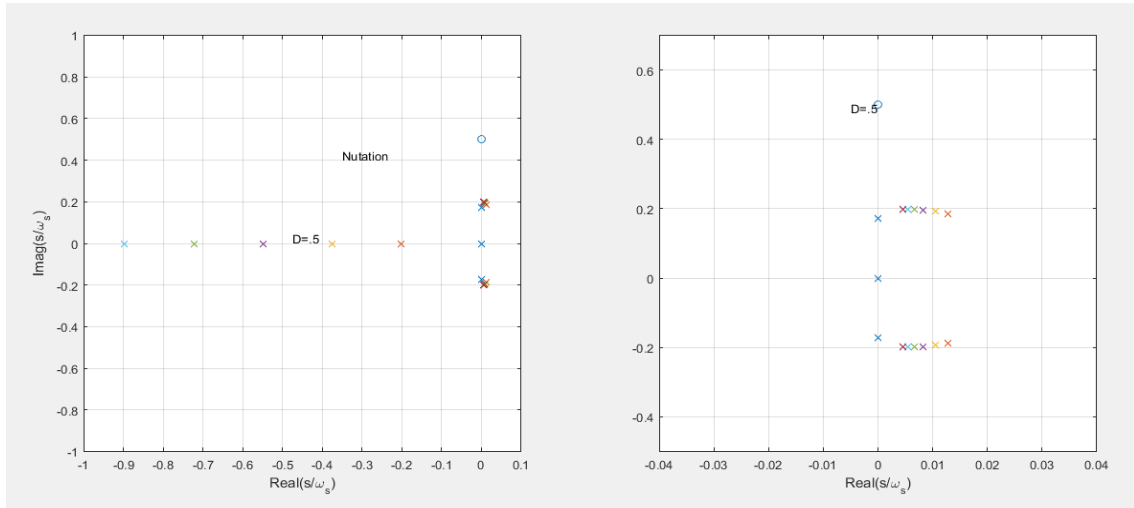


Figure 5.5 Root locus vs damping constant D for rod-like spacecraft with nutation damping wheel.

For rod-shaped spacecraft, $I_S < I_T$, which implies $(\lambda - 1)^2 < z^2$, that is, the zero of the root locus is above the nutation pole; a root locus versus D . Figure 5.5 shows that the spacecraft is *destabilized*. As the poles are identified in right hand side of the S-plane.

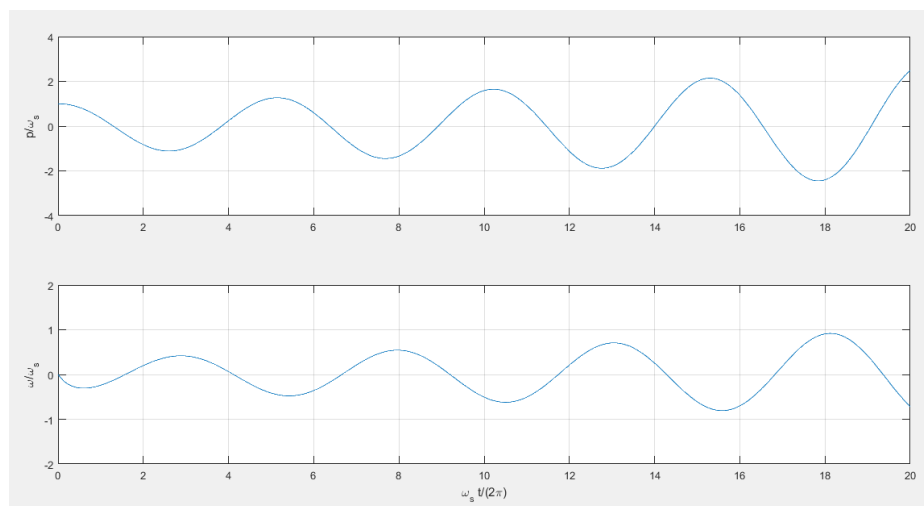


Figure 5.6. Response of rod-like spacecraft with nutation damping wheel to an impulsive roll disturbance torque

Figure 5.6 shows the response of a rod-like spacecraft to an impulsive roll disturbance torque for the case $\lambda=.8$, $\epsilon = .06$, $D = .5$. In which the angular velocity of the damper wheel, ω keeps on oscillating, which shows that the damper wheel is not stable.

Since no real body is actually rigid, energy dissipation due to structural deformations will cause structural damping. Many spacecraft carry liquid rocket fuel, and as this fuel is used up, fuel sloshing will occur, which also dissipates energy. It is evident from the preceding discussion that single-spin spacecraft can be spin stabilized passively only about a major axis.

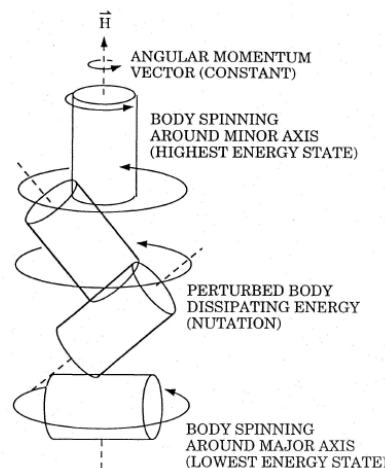


Figure 5.7 Instability of a spacecraft when spun about its minor axis

From the energy viewpoint, a body spinning about its minor axis has maximum rotational energy; energy dissipation causes the total energy to decrease until the body has minimum rotational energy, which corresponds to spin about the body's major axis. This is explained in Figure 5.7.

Nutation damping is having a constrain. Because with this a satellite can only be operated stable in major axis. Even a disc shaped satellite with booster attached will makes a rod-like shape.to avoid this a damper has to be placed on a de-spun part of the spacecraft. This enables it to spin stabilized passively about a minor axis. For this dual spin stabilization method is preferred.

The advantage of using spin stabilization control is, it is a very simple way to keep the spacecraft pointed in a certain direction, which can be used in case of communication satellites. The spinning spacecraft resists perturbing forces, which tend to be small in space, just like a gyroscope or a top. A disadvantage to this type of stabilization is that the satellite cannot use large solar arrays to obtain power from the Sun. Thus, it requires large amounts of battery power. Another disadvantage of spin stabilization is that the instruments or antennas also must perform “despin” maneuvers so that antennas or optical instruments point at their desired targets

6 Attitude Control with a Gimballed Momentum Wheel

6.1.Introduction

Spin with nutation damping is the easiest way to stabilize the spacecraft attitude, but the direction of spin axis shifts when an external disturbance torque acts on the spacecraft. To keep the spacecraft attitude in a desired orientation at all times with a greater precision without using any fuel, a gimballed momentum wheel (GMW) can be used. It can be also called as Control Moment Gyro (CMG).

CMGs differ from reaction wheels. The latter apply torque simply by changing rotor spin speed, but the former tilt the rotor's spin axis without necessarily changing its spin speed. CMGs are also far more power efficient. For a few hundred watts and about 100 kg of mass, large CMGs have produced thousands of newton meters of torque. A reaction wheel of similar capability would require megawatts of power [11].

	Reaction wheels	SGCMG	DGCMG
Hardware complexity	Simple	Complex	Very complex
Algorithms	Simple	Very complex	Complex
Output torque	small	Big	Big
Miniaturization	Possible	Possible	impossible

Table 6.1.Comparison of reaction wheels, Single Gimbal Control Moment Gyroscope and Double gimbal control moment gyroscope

As an actuator of spacecraft attitude control, Control Moment Gyroscope (CMG) produces significant output torque and exhibits excellent control linearity, anti-disturbance, and rapid response features. Therefore, CMG is the preferred actuator for long-life spacecraft. The CMG achieves spacecraft attitude change through the angular momentum change of the flywheel which is forced by frame rotation.

6.2 Single-gimbal momentum wheel

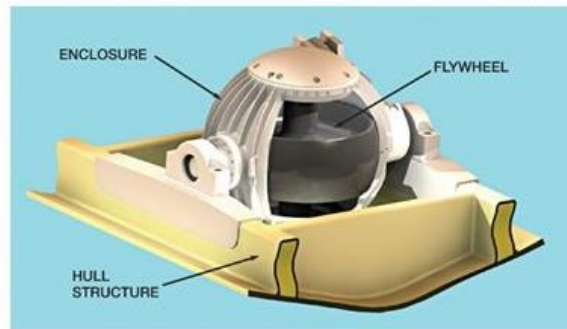


Figure 6.1. Single Gimbal Control Moment Gyroscope

The most efficient CMGs only a single gimbal wheel. When the gimbal of this type CMG rotates, the change in direction of angular momentum of rotor denotes a torque that reacts onto the body to which the CMG is mounted, e.g. a spacecraft. Except for effects due to the motion of the spacecraft, this torque is due to a constraint, so it does no mechanical work. Single-gimbal CMGs exchange angular momentum in a way that requires very little power, with the result that they can apply very large torques for minimal electrical input.

6.3 Dual-gimbal

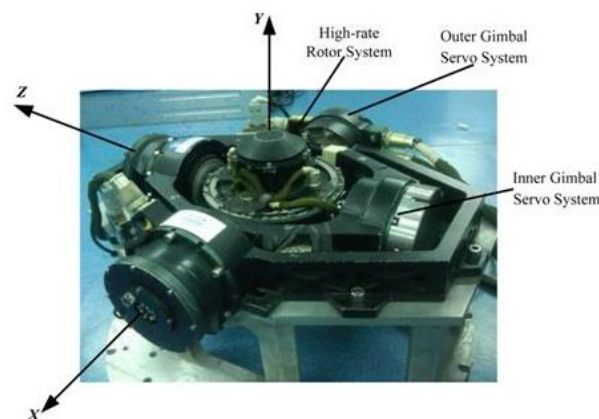


Figure 6.2. Double Gimbal Control Moment Gyroscope with outer and inner servo system

Such a CMG includes two gimbals per rotor. As an actuator, it is more versatile than a single-gimbal CMG because it is capable of pointing the rotor's momentum vector in any direction. However, the torque generated by one gimbal's motion must often be reacted by the other gimbal on its way to the spacecraft, requiring more power for a given torque than a single-gimbal CMG.

The problem with reaction wheels is that it doesn't work well with larger spacecraft. A reaction wheel has to spin so fast as the mass (moment of Inertia) of the spacecraft increases. In the case of massive objects like the International Space Station, the gyroscopic effects from the control moment gyros are preferred to control the spacecraft.

A momentum flywheel with the 3-axis controlled magnetic bearing displays good performance for attitude control of satellite with biased momentum [12].

Unlike reaction wheels, the CMGs already have an initial angular momentum in it, which is controlled by the primary motor. The spacecraft is balanced by another CMG in the opposite direction, orthogonal to each other. Besides this, the internal setup is quite different from a reaction wheel too. The flywheel of a CMG will be inside a gimbal mount, free to be rotated about an axis. When a secondary motor is attached to that gimbal axis, one can apply torque to the spinning flywheel at a different axis.

So when the spacecraft needs to be re-oriented to a new attitude, the secondary motors applies torque and change the axis of rotation of the flywheel. The gyroscopic effect kicks in and applies a torque on the spacecraft at ninety degrees equal to the torques acting on the gyroscope [13].

6.4 Control Concept :

In this section, the fast control concept using two-gimbal momentum wheel (GMW), which provides 3-axis attitude control has been considered (Figure 6.3). The angular momentum imparted to the spacecraft by the external disturbances can be transferred to the GMW by torquing the two gimbals, which changes the direction of the spin axis and the wheel itself, which changes the spin rate.

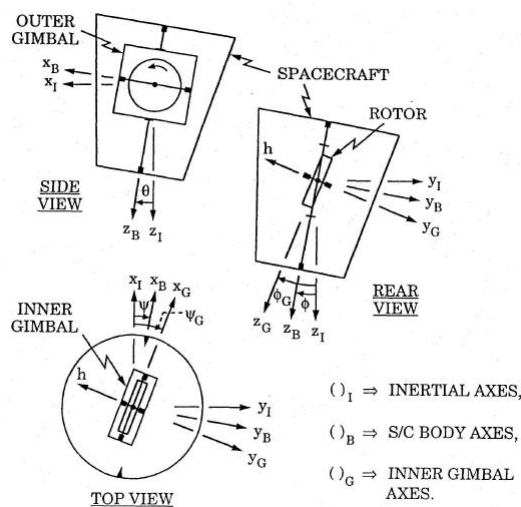


Figure 6.3.Spacecraft with gimbaled momentum wheel (GMW)

The external disturbance torques are counteracted by the internal torques on GMW gimbal cause the direction of spin axis of the GMW rotor drift. Thus if the external disturbance torque is zero and GMW spin angular momentum is large enough, the GMW spin axis direction deviates only through small angle from its nominal direction. If constant angular momentum is transferred to a GMW because of the constant disturbances, the wheel axis gradually lines up with the direction of this torque and wheel speed increases steadily. For this external torque provided by thrusters must be fired to de-saturate the GMW [4].

6.4.1 Equations of Motion of the Spacecraft

For the design of attitude control using gimballed wheel, the equations of motion of non-spinning spacecraft with external disturbances are considered

$$I_x \dot{p} \cong Q_{cx} + Q_{dx} \quad (6.1)$$

$$\dot{\phi} \cong p \quad (6.2)$$

$$I_y \dot{q} \cong Q_{cy} + Q_{dy} \quad (6.3)$$

$$\dot{\theta} \cong q \quad (6.4)$$

$$I_z \dot{r} \cong Q_{cz} + Q_{dz} \quad (6.5)$$

$$\dot{\psi} \cong r \quad (6.6)$$

which are reasonable approximations for small angles. Here Q_c is the control torque and Q_d is the external disturbance torque. (Q_{cx}, Q_{cz}) are applied to the spacecraft from the inner and outer gimbals, Q_{cy} by a motor on the wheel axis

6.4.2 Equations of motion of Gimballed momentum wheel with two gimbals

Consider the Euler angles of the inner gimbal with respect to the inertial space be $[\phi_G, \theta_G, \psi_G]$ and let the angular velocity of the inner gimbal with respect to inertial space be $[p_G, q_G, r_G]$. Then the angular momentum of GMW is then

$$\vec{H} = [J_x p_G, J_y q_G - h, J_z r_G] \quad (6.7)$$

where

$$h = 2J_\omega \omega_s = \text{spin angular momentum of rotor,}$$

$$J_x = J_\omega + J_{IGx},$$

$$J_y = J_\omega + J_{IGy} + J_{OGy},$$

$$J_z = J_\omega + J_{IGz} + J_{OGz},$$

J_ω = moment of inertia of inertia wheel about a diameter

J_{IG} = Moment of inertia of inner gimbal

J_{OG} = Moment of inertia of outer gimbal

From Euler's law,

$\vec{H}_I = \vec{H}_G + \vec{\omega}_G * \vec{H} = \vec{Q}$, which is an equation of angular momentum conservation law. The torque can be created by accelerating or decelerating the angular momentum.

it follows that

$$J_x \dot{p}_G + h r_G = -Q_{cx}, \quad (6.8)$$

$$J_y \dot{q} - \dot{h} = Q_{cy}, \quad (6.9)$$

$$J_z \dot{r}_G - h p_G = -Q_{cz}, \quad (6.10)$$

and, for small angles

$$\dot{\phi}_G \cong p_G \quad (6.11)$$

$$\dot{\theta}_G \cong q_G \quad (6.12)$$

$$\dot{\psi}_G \cong r_G \quad (6.13)$$

Here, only the coupling actions for roll and yaw motions are discussed, as the pitch motions are uncoupled from roll/yaw motions for small angle deviations.

6.4.3 Equations of Roll/Yaw system

The roll and yaw motions of GMW are coupled by the spin angular momentum, h in equations (8) and (10). The roll and yaw motions of GMW are coupled to the roll and yaw motions of spacecraft by the control torques (Q_{cx}, Q_{cz}), since the torque of spacecraft produces an equal and opposite torque on GMW:

$$I_x \ddot{\phi} \cong Q_{cx} + Q_{dx} \quad (6.14)$$

$$I_z \ddot{\psi} \cong Q_{cz} + Q_{dz} \quad (6.15)$$

$$J_x \ddot{\phi}_G + h \dot{\psi}_G \cong -Q_{cx} \quad (6.16)$$

$$J_z \ddot{\psi}_G - h \dot{\phi}_G \cong -Q_{cz} \quad (6.17)$$

Adding (14) to (16) and (15) to (17) eliminates the control torques :

$$J_x \dot{\phi}_G + h\psi_G + I_x \dot{\phi} \triangleq H_x \quad (6.18)$$

$$\dot{H}_x = Q_{dx} \quad (6.19)$$

$$J_z \dot{\psi}_G + h\phi_G + I_z \dot{\psi} \triangleq H_z \quad (6.20)$$

$$\dot{H}_z = Q_{dz} \quad (6.21)$$

Equations (18)–(21) imply ,for a stable control ($\dot{\phi}_G \rightarrow 0, \dot{\psi}_G \rightarrow 0$) that impulsive disturbance torques yield

$$h\psi_G \rightarrow H_x \quad (6.22)$$

$$H_x = \int_0^t Q_{dx} dt \quad (6.23)$$

$$-h\phi_G \rightarrow H_z \quad (6.24)$$

$$H_z = \int_0^t Q_{dz} dt \quad (6.25)$$

That is, the roll and yaw components of the total spacecraft angular momentum are transferred to the gimbaled momentum wheel.

For the roll/yaw control, an horizon sensor is needed to measure ϕ , rate gyros to measure (p, r), and sensors on the outer gimbal to measure $\phi - \phi_G$ and $\psi - \psi_G$. Using the ϕ, p, r measurements, ψ can be estimated using the “orbital gyro-compassing”

6.4.4 Passive Roll/Yaw stabilization

First the passive stabilization control of yaw and roll motions are discussed in this section.

For passive roll and yaw attitude control, viscous dampers can be used. A general industrial and commercial standard for durability and efficiency is to maintain torsional vibration within < 0.2 degrees peak twist. To accomplish this the design is composed of three main components:

1. Outer Housing
2. Inner Inertia Ring
3. Viscous Fluid

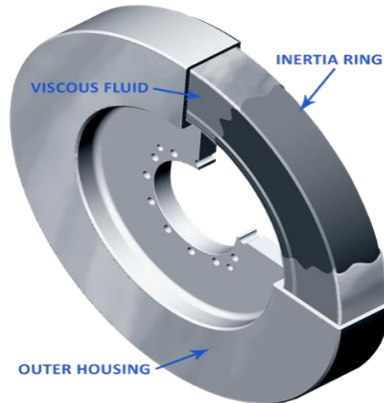


Figure 6.4 Viscous damper

The outer housing is directly connected to the shaft and moves with shaft rotation. Inside the inner inertia ring freely rotates in a thin layer of viscous fluid. As a vibration event happens it causes the outer housing and inner inertia ring to rotate independently at different speeds. The resulting shear action through the viscous fluid diminishes the vibration by transforming it to heat [14].

The passive stabilization of satellite roll and yaw attitude can be obtained by connecting the gimbals to the spacecraft with the viscous dampers

$$\begin{aligned} Q_{cx} &= -D(\dot{\phi} - \dot{\phi}_G) \\ Q_{cz} &= -D(\dot{\psi} - \dot{\psi}_G) \end{aligned} \quad (6.26)$$

Equations (19) and (22) are quadratures for finding (H_x, H_z) . (16) - (20) and (22) are four equations for $(\phi_G, \psi_G, \phi, \psi)$ given (H_x, H_z) . The characteristic equation of that damped system shows that for $J \leq I_x I_z$, there are two complex modes with Eigen values differ by several orders of magnitude.

For $J_x = J_z = J$ the faster set eigen values is

$$s_3, s_4 \cong \frac{D}{J} \pm \frac{h}{J} j \quad (6.27)$$

Which corresponds to a damped nutation modes. The other mode may be analysed by treating the nutation mode as quasi-steady, that is, by putting $J_x = J_z = 0$ in (18) and (19). Thus, if we

use time in units of I_x/h , (H_x, H_z, D) in units of h/I_z in units of I_x , thus we obtain equations of motion as

$$\begin{aligned}\dot{\phi}_G &= \frac{D}{(1+D^2)I_z} [\phi_G] + \frac{D^2}{(1+D^2)} [\psi_G] + \frac{D^2}{(1+D^2)} [H_x] + \frac{D}{(1+D^2)I_z} [H_z] \\ \dot{\psi}_G &= \frac{D^2}{(1+D^2)I_z} [\phi_G] + \frac{D}{(1+D^2)} [\psi_G] + \frac{D}{(1+D^2)} [H_x] + \frac{D^2}{(1+D^2)I_z} [H_z] \\ \dot{\phi} &= -\psi_G + H_x \\ \dot{\psi} &= \frac{1}{I_z} [\phi_G] - \frac{1}{I_z} [H_z]\end{aligned}$$

Consider $\mu=D/(1+D^2)$.

Then the state space representation of above equations of motion are

$$\begin{bmatrix} \dot{\phi}_G \\ \dot{\psi}_G \\ \dot{\phi} \\ \dot{\psi} \end{bmatrix} \cong \begin{bmatrix} \frac{\mu}{I_z} & \mu D & 0 & 0 \\ \frac{\mu D}{I_z} & -\mu & 0 & 0 \\ 0 & -1 & 0 & 0 \\ \frac{1}{I_z} & 0 & 0 & 0 \end{bmatrix} \begin{bmatrix} \phi_G \\ \psi_G \\ \phi \\ \psi \end{bmatrix} + \begin{bmatrix} \mu D & -\frac{\mu}{I_z} \\ \mu & \frac{\mu D}{I_z} \\ 1 & 0 \\ 0 & -\frac{1}{I_z} \end{bmatrix} \begin{bmatrix} H_x \\ H_z \end{bmatrix} \quad (6.28)$$

The characteristic equation of (6.28) is

$$s^2 \left[s^2 + \mu \left(1 + \frac{1}{I_z} \right) s + \mu^2 (D^2 + 1/I_z) \right] = 0 \quad (6.29)$$

For this special case $I_z = 1$, eigen values are

$$S=(0,0,-\mu \pm \mu D j) . \quad (6.30)$$

The *asymptotic response* of the damped system to a roll or yaw *disturbance* torque impulse may be obtained from (30):

$$\begin{bmatrix} \phi \\ \psi \\ \phi_G \\ \psi_G \end{bmatrix} \rightarrow \begin{bmatrix} \frac{1}{D} & -\frac{1}{h} \\ \frac{1}{h} & \frac{1}{D} \\ 0 & -\frac{1}{h} \\ \frac{1}{h} & 0 \end{bmatrix} \begin{bmatrix} H_x \\ H_z \end{bmatrix},$$

(6.31)

Where (H_x, H_z) are the roll and yaw disturbance torque impulse magnitudes. Thus the torque impulse is transferred to the GMW.

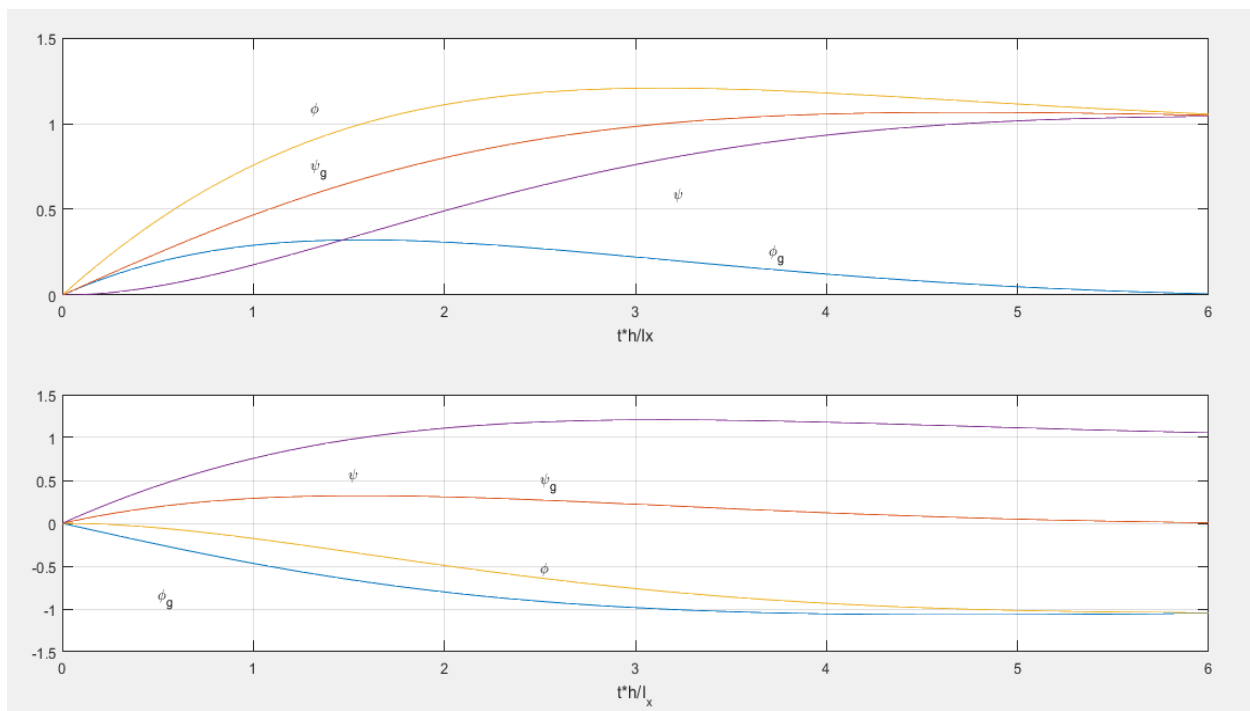


Figure 6.5. Response of S/C with a GMW with passive control of GMW to impulsive roll and yaw disturbance torques with viscous damper between S/C and outer gimbal

Figure 6.5 shows the response to impulsive roll and yaw disturbance torques that produce steps in (H_x, H_z) of magnitude h for the case $D = h, I_z = I_x$. Hence the impulses of the torque will be transferred to the GMW, but (ϕ, ψ) have the offsets depend on D and h . If D and H are large compared to the anticipated values of H_x and H_z , then the offset angles are small. This system can be considered for a backup system.

To bring (ϕ, ψ) to zero after an impulsive disturbance torque, active control must be considered, which requires (ϕ, ψ) sensors and torque actuators on the outer gimbal of GMW

6.4.5 Active Roll/Yaw control

A Passive gimbal damper has to be used in case of an active roll/yaw control. The passive gyroscopic damper (PGD) has a rotor in the gimbal rotating at a constant angular velocity. The gimbal is driven by a gyroscopic moment induced by the rotation of the main system, and is passively controlled by the torsional spring and the viscous damper around the gimbal axis. The gimbal rotation again induces the resistive gyroscopic moment against the excitation. The mechanism enables effective vibration control compared with conventional dynamic vibration absorbers, while it has a rather simple structure. Design methods for typical design conditions are developed that give the optimal gimbal spring and the optimal gimbal damper for a given rotor and rotor speed [15].

These passive gimbal dampers are combined with the active feedback of (ϕ, ψ) as follows:

$$Q_{cx} = -D(\dot{\phi} - \dot{\phi}_G) - K\phi, \quad (6.32)$$

$$Q_{cz} = -D(\dot{\psi} - \dot{\psi}_G) - K\psi, \quad (6.33)$$

that is, restoring springs are supplied in roll and yaw to the desired attitude. This requires (ϕ, ψ) sensors and torque actuators on the outer gimbal. Again, the damping torques are large compared to the D' Alembert torques on the outer gimbal, so we put $J_x = J_z = 0$. Considering the same normalization of variables as in (30), the state space equations of motion are

$$\begin{aligned} \dot{\phi}_G = & \frac{D}{(1+D^2)I_z} [\phi_G] + \frac{D^2}{(1+D^2)} [\psi_G] + \frac{DK}{(1+D^2)} [\phi] - K[\psi] + \frac{D^2}{(1+D^2)} [H_x] \\ & + \frac{D}{(1+D^2)I_z} [H_z] \end{aligned}$$

$$\begin{aligned} \dot{\psi}_G = & \frac{D^2}{(1+D^2)I_z} [\phi_G] + \frac{D}{(1+D^2)} [\psi_G] + K[\phi] + \frac{DK}{(1+D^2)} + \frac{D}{(1+D^2)} [H_x] \\ & + \frac{D^2}{(1+D^2)I_z} [H_z] \end{aligned}$$

$$\dot{\phi} = -\psi_G + H_x$$

$$\dot{\psi} = \frac{1}{I_z} [\phi_G] - \frac{1}{I_z} [H_z]$$

State space representation of above equation is given by

$$\begin{bmatrix} \dot{\phi}_G \\ \dot{\psi}_G \\ \dot{\phi} \\ \dot{\psi} \end{bmatrix} \cong \begin{bmatrix} \frac{\mu}{I_z} & \mu D & \mu K & -k \\ \frac{\mu D}{I_z} & -\mu & K & \mu K \\ 0 & -1 & 0 & 0 \\ \frac{1}{I_z} & 0 & 0 & 0 \end{bmatrix} \begin{bmatrix} \phi_G \\ \psi_G \\ \phi \\ \psi \end{bmatrix} + \begin{bmatrix} \mu D & -\frac{\mu}{I_z} \\ \mu & \frac{\mu D}{I_z} \\ 1 & 0 \\ 0 & -\frac{1}{I_z} \end{bmatrix} \begin{bmatrix} H_x \\ H_z \end{bmatrix}$$

(6.34)

where $\mu = D / (1 + D^2)$ and K is in units of h^2/I . For $D=1, I_z=1$ are considered

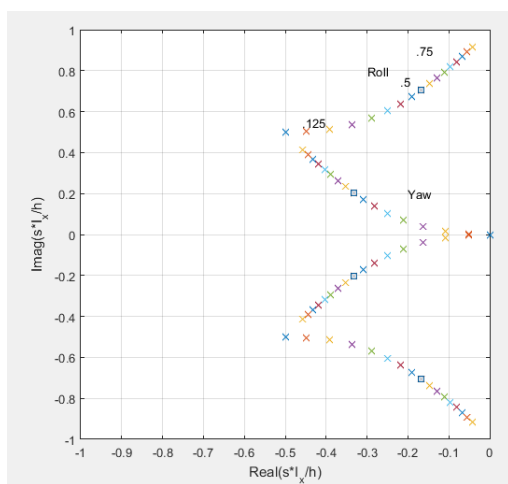


Figure 6.6.1. Normalization 1

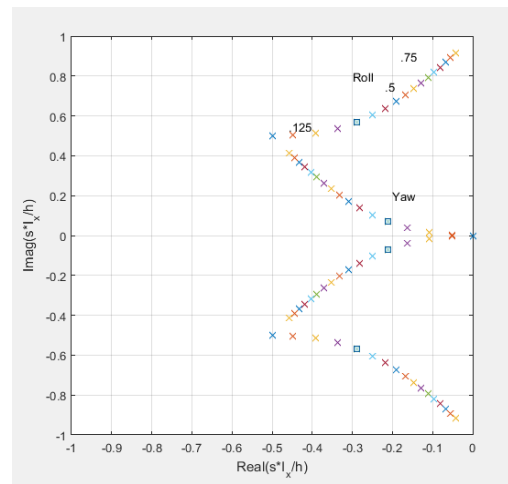


Figure 6.6.2 Normalization 2

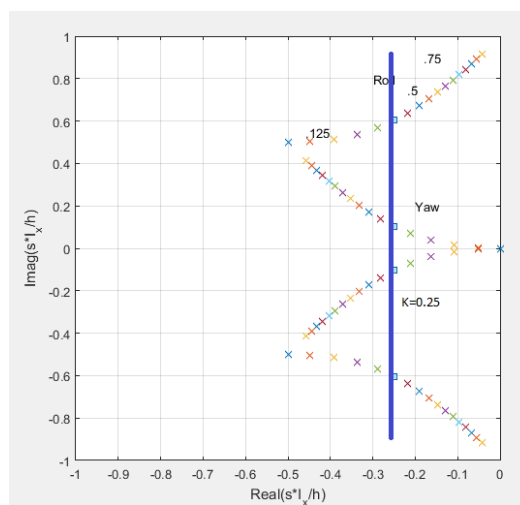


Figure 6.6.3 Normalization 3

Figure 6.6 Locus of closed-loop poles vs K for active control of S/C with a GMW

Figure 6.6 is the locus of the closed-loop roots versus K for the case $D = h$, $I_z = I_x$. The two poles at the origin are stabilized while the damping of the other two poles is reduced; a good value of normalized K is .25 where the real parts of the two sets of complex poles are equal at - .25. Hence, a proportional controller with the K gain value of 0.25 is designed for the active control of S/C with a GMW

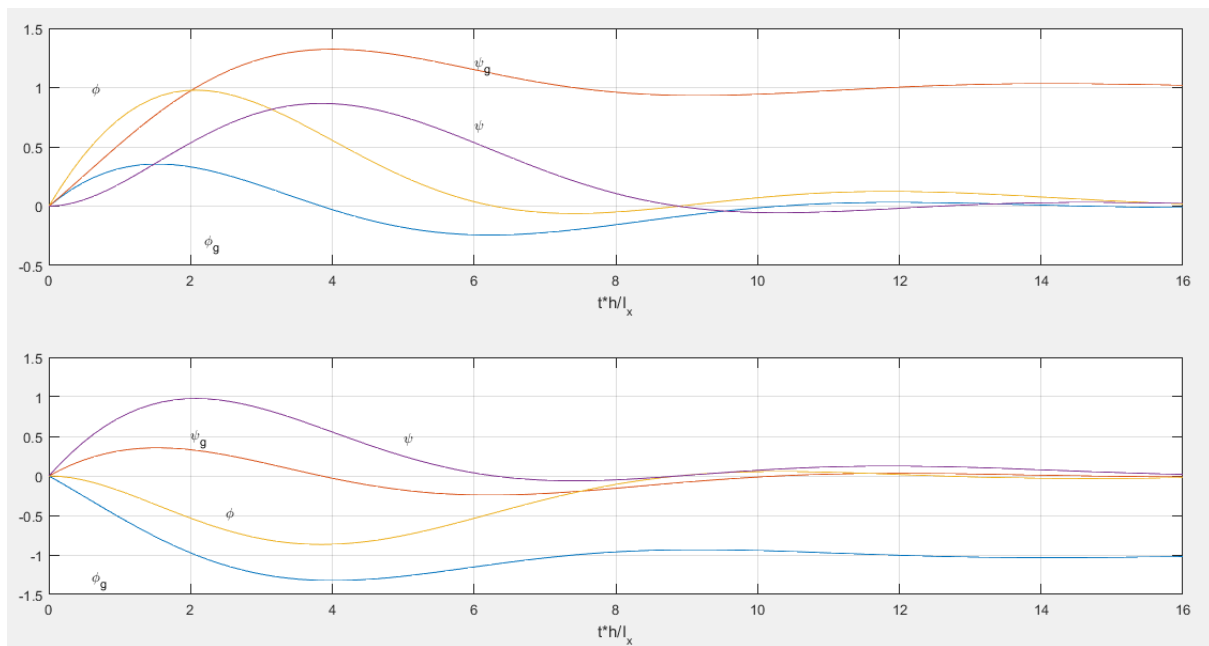


Figure 6.7 Response of S/C with active control of a GMW to impulsive roll and yaw disturbance torques.

Figure 6.7 shows the response of the spacecraft with the active control of GMW to impulsive roll and yaw disturbance torques. Comparing with the passive control the values of (ϕ, ψ) are returned to zero in active control ; this is done by over-transferring angular momentum to the GMW from the spacecraft, then using the excess to bring the S/C attitude back to zero. Figure 6.7 validates the attitude control of spacecraft with the GMW.

This system has the advantage that ,even if the active system fails ,the spacecraft will remain close to the desired attitude with the dampers alone, which fairly acts as a good back-up system.

7. Attitude control during thrust maneuvers

7.1 Introduction

Spacecraft attitude has to be controlled during translational thrusting maneuvers in terms of accuracy specifications determined by the mission. Desired velocity changes can be realized by long burns at low thrust levels or relatively short burns at high thrust levels. Low thrust levels generally result in relatively minor additions to the disturbance torques affecting vehicle orientation. However, the propulsive force more often is high, and the line of action of the force is generally offset from the centre of mass by an amount that is uncertain and changing.

The result can be a large disturbance torque whose presence is important to and often dominates the design of the attitude-control system. The dynamic characteristics of the attitude-control system can have a significant influence on the accuracy and efficiency with which thrusting maneuvers can be performed [16].

The attitude-control system shall be capable of the following:

1. Sustaining thrust-vector pointing accuracy, in the presence of all anticipated disturbances, within the tolerance limit of the mission requirement.
2. Damping initial transients, which result from off-nominal conditions or thruster misalignment without exceeding structural load limits or adding significantly to the thrust vector error.

The thrust misalignment torque is much bigger than that of the external disturbance torque due to the availability of solar pressure, earth's magnetic fields, and gravity. Hence, an attitude control system is required. It can be performed using reaction jets, Gimbaled engine and with the off modulation of a multi-nozzle main engine.

Control using the reaction jets usually consists of switching on-off characteristics and the synthesis of time-variant control logic is considered more complicated. Reaction jets sized to handle disturbances with the main engine off do not have enough torque to overcome the thrust misalignment torque. Whereas, using the off-modulation engine with three nozzles, where each nozzle is switched on and off for controlled periods. This method is attractive only for the unmanned missions as it avoids the engine and an active control system.

In the section, attitude control during thrust maneuvers using a Gimbaled engine is considered.

7.2 Attitude control during thrust maneuvers using a Gimbaled engine

In a gimbaled thrust system, the exhaust nozzle of the rocket can be turned around a point or axis from side to side. As the nozzle is moved, the direction of the thrust is changed relative to the centre of gravity of the rocket. Figure 7.1 shows three cases.

On the rocket at the left, the nozzle has been deflected to the left and the thrust line is now inclined to the rocket centre line at an angle α called the gimbal angle. Since the thrust no longer

passes through the centre of gravity, a torque is generated about the centre of gravity and the nose of the rocket turns to the left. If the nozzle is gimbaled back along the centre line, the rocket will move to the left. The middle rocket shows the "normal" flight configuration in which the direction of thrust is along the centre line of the rocket and through the centre of gravity of the rocket. The third rocket at the right shows that the nozzle has been deflected to the right and the nose is moved to the right.[17]

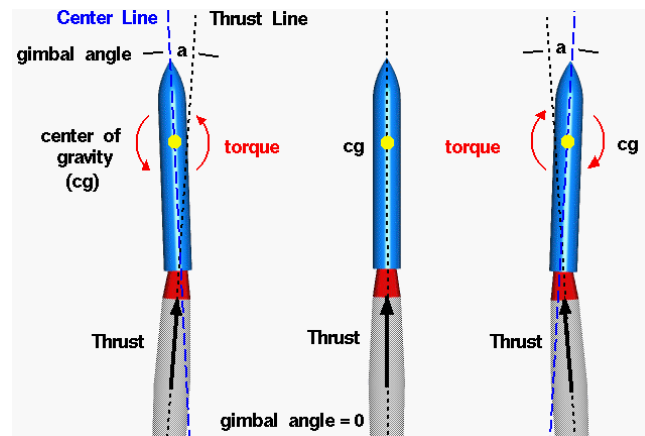


Figure 7.1 Nozzle movement with respect to the centre line during flight [2]

Reaction jets assigned to handle the turbulences with the main engine off do not have enough torque to overcome the thrust misalignment torque. Hence, a special additional reaction jet system is required. To avoid this, some spacecraft launch vehicles have used a gimbaled main engine for attitude control. Fig. 7.2 shows a system for controlling pitch motions .

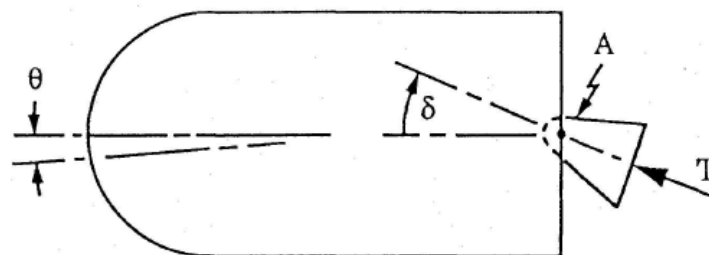


Figure 7.2 Spacecraft with a gimbaled main engine for pitch motion control

To synthesize control logic for this two rigid-body system, we need the equations of motion with a control torque on the gimbal axis. Equations are developed using D' Alembert's method. Fig. 7.3 shows free-body diagrams of the spacecraft and the nozzle with the internal control

torque Q and the internal forces X and Z that act on the gimbal axis. Also shown are the D'Alembert forces and torques and the thrust force T .

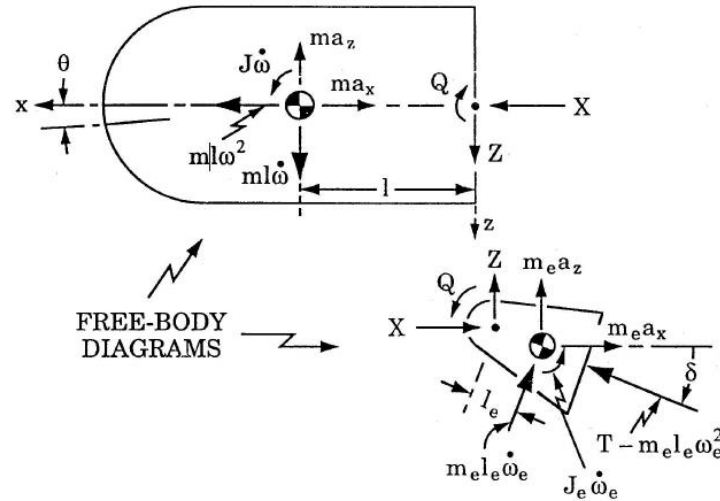


Figure 7.3 Spacecraft with a gimbaled main engine

Taking moments about the gimbal axis (A in the diagrams), the equations of motion for the spacecraft are

$$0 = \sum M_A = (J + ml^2)\dot{\omega} - ma_z l - Q, \quad (7.1)$$

$$0 = \sum F_z = -ma_z + ml\dot{\omega} + Z, \quad (7.2)$$

$$0 = \sum F_x = -ma_x + ml\omega^2 + X. \quad (7.3)$$

The equations of motion for the gimbaled engine are

$$0 = \sum M_A = (J_e + m_e l_e^2)\dot{\omega}_e + m_e a_z l_e \cos \delta + m_e a_x l_e \sin \delta + Q, \quad (7.4)$$

$$0 = \sum F_z = -m_e a_z - m_e l_e \dot{\omega}_e \cos \delta - [T - m_e l_e \omega_e^2] \sin \delta - Z, \quad (7.5)$$

$$0 = \sum F_x = -m_e a_x - m_e l_e \dot{\omega}_e \cos \delta - [T - m_e l_e \omega_e^2] \cos \delta - X, \quad (7.6)$$

and

$$\dot{\delta} = \omega_e - \omega, \quad (7.7)$$

where

(ω, ω_e) = angular velocity of (spacecraft, engine),

(m, m_e) = mass of (spacecraft, engine),

(J, J_e) = moment of inertia about c.m. of (spacecraft, engine),

(a_x, a_z) = spacecraft body-axes components of acceleration of gimbal axis (point A)

Eliminating X between (3) and (6), and Z between (2) and (4), gives the acceleration components:

$$(m + m_e)a_x = ml\omega^2 - (m_e l_e (\omega_e^2 \cos \delta + \dot{\omega}_e \sin \delta) + T \cos \delta), \quad (7.8)$$

$$(m + m_e)a_z = ml\omega^2 - (m_e l_e (-\omega_e^2 \sin \delta + \dot{\omega}_e \sin \delta) - T \sin \delta). \quad (7.9)$$

Substituting for (a_x, a_z) from (8) and (9) into (1) and (4) and repeating (7) gives the following equations of motion :

$$J^* \dot{\omega} + J_c (\dot{\omega}_e \cos \delta - \omega_e^2 \sin \delta) = Q - b \sin \delta, \quad (7.10)$$

$$J_e^* \dot{\omega}_e + J_c (\dot{\omega} \cos \delta + \omega^2 \sin \delta) = -Q, \quad (7.11)$$

$$\dot{\delta} + \omega - \omega_e = 0, \quad (7.12)$$

where

$$J^* \triangleq J + m^* l^2,$$

$$J_e^* \triangleq J_e + m^* l_e^2,$$

$$J_c \triangleq m^* l l_e,$$

$$m^* \triangleq m m_e / (m + m_e),$$

$$b \triangleq m l T / (m + m_e).$$

The equations of motion may be linearized for $|\delta| \ll 1, J_c \omega_e^2 \ll b$ and $J_c \omega^2 \ll b$. Taking the laplace transform of these equations gives

$$\begin{bmatrix} J^* s & J_c s & b \\ J_c s & J_e^* s & 0 \\ 1 & -1 & s \end{bmatrix} \begin{bmatrix} \omega(s) \\ \omega_e(s) \\ \delta(s) \end{bmatrix} \cong \begin{bmatrix} 1 \\ -1 \\ 0 \end{bmatrix} Q(s). \quad (7.13)$$

From (13), we may deduce the transfer function from Q to ω :

$$\frac{\omega(s)}{Q(s)} = \frac{p^2}{bs} \frac{s^2 + z^2}{s^2 - p^2}, \quad (7.14)$$

where

$$z^2 \triangleq \frac{b}{J_e^* + J_c}, \quad (7.15)$$

$$p^2 \triangleq b(J_e^* + J_c)/(J_e^* J_e^* - J_c^2) \quad (7.16)$$

Since $\omega - \dot{\theta}$ (14) may be written as

$$\frac{\theta(s)}{Q(s)} = \frac{1}{s^2} \frac{s^2 + z^2}{s^2 - 1} \quad (7.17)$$

where time is in units of $1/p$, z in units of p , and Q in units of b . Note the zeros of this transfer function on the imaginary axis imply that torquing the engine at this frequency would produce no pitch motion of the spacecraft .

With (ω, ω_e) in units of p , time in units of $1/p$, and Q in units of b , then state equation of (13) is given as

$$\begin{aligned} \dot{\omega} &= -\frac{J_e^*}{J_e^* + J_c} \delta + Q, \\ \dot{\omega}_e &= \frac{J_c}{J_e^* + J_c} \delta - \frac{J_e^* + J_c}{J_e^* - J_c} Q, \\ \dot{\delta} &= -\omega + \omega_e \\ \dot{\theta} &= \omega \end{aligned}$$

and the state-variable form is given as

$$\begin{bmatrix} \dot{\omega} \\ \dot{\omega}_e \\ \dot{\delta} \\ \dot{\theta} \end{bmatrix} \cong \begin{bmatrix} 0 & 0 & -\epsilon & 0 \\ 0 & 0 & 1 - \epsilon & 0 \\ -1 & 1 & 0 & 0 \\ 1 & 0 & 0 & 0 \end{bmatrix} \begin{bmatrix} \omega \\ \omega_e \\ \delta \\ \theta \end{bmatrix} + \begin{bmatrix} 1 \\ -\lambda \\ 0 \\ 0 \end{bmatrix} Q, \quad (7.18)$$

where

$$\begin{aligned} \epsilon &\triangleq J_e^*/(J_e^* + J_c), \\ \lambda &\triangleq (J_e^* + J_c)/(J_e^* - J_c) \end{aligned}$$

Considering $m_e = \frac{m}{30}$, $l_e = \frac{l}{10}$, $J = \frac{ml^2}{3}$, $J_e = m_e l_e^2/3$, which gives

$$\epsilon = 0.11851$$

$$\lambda = 100.78$$

$$Z = 3.3260$$

Using linear-quadratic synthesis with performance index

$$J = \int_0^{\infty} (A\theta^2 + Q^2) dt, \quad (7.19)$$

Weighting factors considered for 1,0.3,0.1,0.03,0.01,0.003,0.001

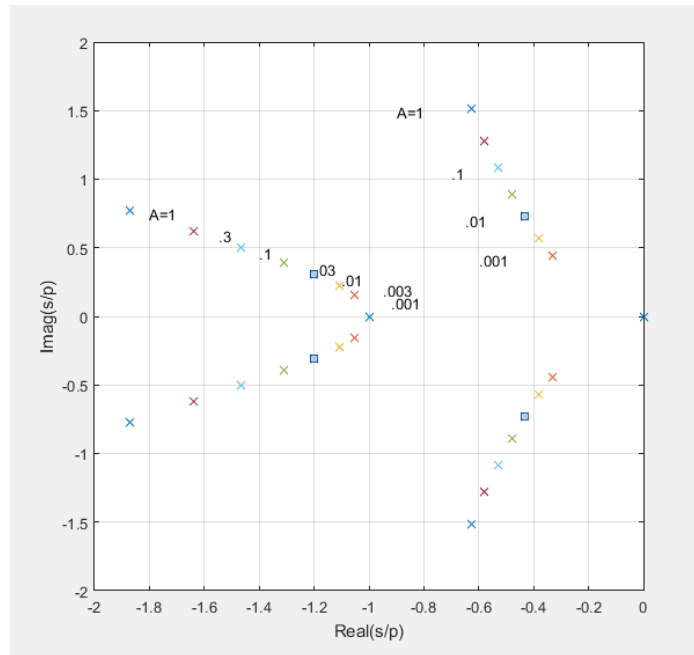


Figure 7.4 Spacecraft with gimballed engine; locus of LQ regulator poles vs weighting factor A

Figure 7.4 shows the locus of the closed-loop poles vs the weighting factor A

Considering A=0.03, the closed loop poles are at

$$s = -0.4801 \pm 0.8908j, -1.31 \pm 0.3925j$$

and the control law, $Q = -K x$ is

$$Q = [-0.4362, +0.0312, +0.0613, -0.1732] \begin{bmatrix} \omega \\ \omega_e \\ \delta \\ \theta \end{bmatrix}$$

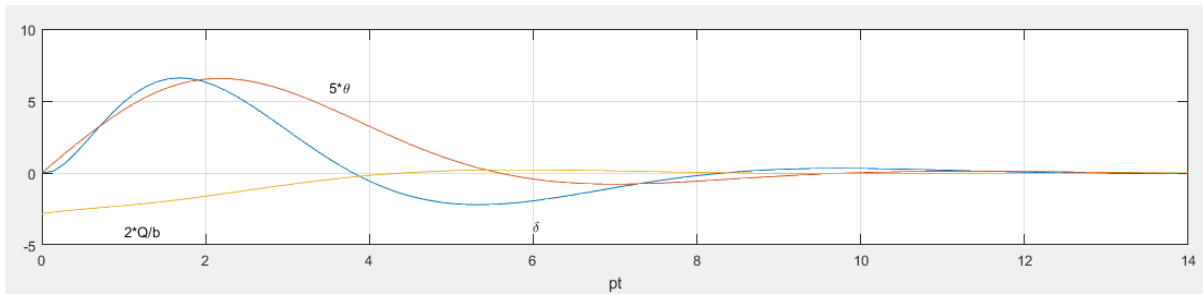


Figure 7.5 Spacecraft with gimbaled engine; response to initial angular velocity

Figure 7.5 shows the response of spacecraft with gimbaled engine to the initial pitch rate. It also shows that the pitch controlling motions deflecting the other control of yaw motion as the forces of pitch and yaw acts on the gimbal axis. The torques about the spacecraft centre of mass add up to zero; that is, the control torque and the torque due to engine deflection are just balanced by the torque due to the reaction force Z.

Advantages of gimbaled engine	Disadvantages of gimbaled engine
<ol style="list-style-type: none"> 1. Provides savings in weight of the spacecraft. 2. Eliminates skewed high thrust control axes due to thruster location on solar panel. 3. Eliminates reaction control coupling with solar panel flexibility. 4. Eliminates flexible plumbing to panel mounted thruster. 5. Eliminates high level thruster valve location problem: <ol style="list-style-type: none"> a) Performance best with thrusters on the tip of solar panels. b) Solar panel temperatures extreme. 6. Simplifies reaction control system mechanization and allows modular design. 7. Makes mission performance less sensitive to centre of mass changes; relaxes centre of mass control requirement. 8. Better growth capability. 	<ol style="list-style-type: none"> 1. Requires actuator development in short time. 2. Needs structural redesign to provide gimbal compatible with: <ol style="list-style-type: none"> a. Space environment. b. Engine heat soak back. 3. Introduces actuator development and qualifications cost as a major addition. 4. Introduces thrust vector control (TVC) coupling with solar panel flexibility.

Table 7.1 Advantage and Disadvantages of using a Gimbaled engine [18]

8 Control of translational motion

8.1 Introduction

In general spacecraft will experience two types of motions. They are translational and rotational motions. Here, only control of translational motions are focussed. The translational motions are controlled by different techniques. The translational motions for a spacecraft with centre of mass are projected by the Newton's equations.

For a spacecraft the external forces acting on it may be divided as control forces \vec{F}_c and other forces \vec{F}_d . Usually these other forces are the disturbances which acts on the spacecraft. This force is equal to $-c\dot{m}$ where $-\dot{m}$ is the rate at which mass is being thrown overboard, and c is the velocity of the mass particles with respect to the spacecraft called "specific impulse". If $|\vec{F}_c| \gg |\vec{F}_d|$, then \vec{F}_d may be considered as a small disturbance and it is called as "fast" control. If $|\vec{F}_c|$ is comparable to $|\vec{F}_d|$, is called as the "slow" control.[4]

Slow control in a circular orbit; in-track/radial is alone considered for thesis purpose.

8.2 Translational motions in space

The natural motions of the centre of mass of a body in space are described by Newton's equations:

$$m\vec{v}^I = \vec{F}, \quad (8.1)$$

$$\dot{\vec{r}}^I = \vec{v}, \quad (8.2)$$

where

m = mass of the spacecraft,

(\vec{v}, \vec{r}) = (velocity, position) of the centre of mass with respect to inertial space

$(\)^I$ = time rate of change with respect to inertial space,

\vec{F} = sum of external forces.

In the absence of external forces, the velocity stays constant, and the position changes linearly with time.

8.3 Translational Motions in Circular Orbit

In circular orbit, centrifugal force balances gravitational force. For *small deviations from circular orbit*, the equations of motion of the centre of mass are conveniently written in locally-horizontal-vertical (LHV) coordinates that rotate with the orbital angular velocity, n (Fig. 8.1):

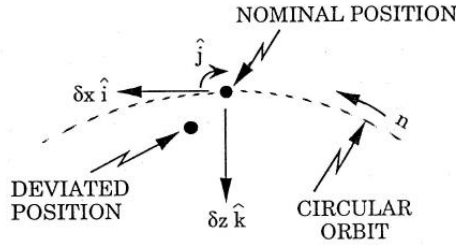


Figure 8.1 Locally-horizontal-vertical (LHV) coordinates for position deviation from circular orbits

$$\delta \vec{v}^I \equiv \delta \vec{v}^L + \vec{\omega}_L \times \delta \vec{v} = \delta \vec{F} / m, \quad (8.3)$$

$$\delta \vec{r}^I = \delta \vec{r}^L + \vec{\omega}_L \times \delta \vec{r} = \delta \vec{v}, \quad (8.4)$$

where

$\delta \vec{v}$ = velocity deviation,

$\delta \vec{r}$ = position deviation

$\delta \vec{F}$ = force deviation,

$()^L$ = denotes time derivative of components with respect to LHV axes,

$\vec{\omega}_L$ = angular velocity of LHV axes with respect to inertial axes.

Following NASA standard notation, δx is in-track position deviation (positive in direction of orbital velocity), δy is cross-track position deviation, and δz is vertical deviation (positive down). Thus,

$$\delta \vec{v} = \hat{i} \delta u + \hat{j} \delta v + \hat{k} \delta w, \quad (8.5)$$

$$\delta \vec{r} = \hat{i} \delta x + \hat{j} \delta y + \hat{k} \delta z, \quad (8.6)$$

$$\vec{\omega}_L = -n \hat{j}, \quad (8.7)$$

where $n \triangleq \sqrt{g/R}$ = orbital angular velocity and $(\hat{i}, \hat{j}, \hat{k})$ are unit vectors along the (x, y, z) axes.

The only force is the inverse-square gravitational force

$$\vec{F} = mg \left(\frac{R}{R-\delta z} \right)^2 \hat{k}, \quad (8.8)$$

where,

g =gravitational force per unit mass at radial distance, R , from the attracting centre.

Thus the deviation in force is given by

$$\delta \vec{F} = 2mg \frac{R^2 \delta z}{(R-\delta z)^3} \hat{k} + mg \left(\frac{R}{R-\delta z} \right)^2 \left(\frac{\partial \hat{k}}{\partial x} \delta x + \frac{\partial \hat{k}}{\partial y} \delta y \right), \quad (8.9)$$

and

$$\frac{\delta \hat{k}}{\delta x} = -\frac{1}{R} \hat{i}, \quad (8.10)$$

$$\frac{\delta \hat{k}}{\delta y} = -\frac{1}{R} \hat{j}. \quad (8.11)$$

Substituting (5)-(7) and (9)-(11) into (1) and (2), we obtain the equations of motion for small deviations from circular orbit. They decouple into a set governing *cross-track motions*

$$\begin{bmatrix} \delta \dot{v} \\ \delta \dot{y} \end{bmatrix} = \begin{bmatrix} 0 & -n^2 \\ 1 & 0 \end{bmatrix} + \begin{bmatrix} T_y/m \\ 0 \end{bmatrix} \quad (8.12)$$

and a set governing *in-track/radial motions*

$$\begin{bmatrix} \delta \dot{u} \\ \delta \dot{w} \\ \delta \dot{x} \\ \delta \dot{z} \end{bmatrix} = \begin{bmatrix} 0 & n & -n^2 & 0 \\ -n & 0 & 0 & 2n^2 \\ 1 & 0 & 0 & n \\ 0 & 1 & -n & 0 \end{bmatrix} \begin{bmatrix} \delta u \\ \delta w \\ \delta x \\ \delta z \end{bmatrix} + \begin{bmatrix} T_x/m \\ T_z/m \\ 0 \\ 0 \end{bmatrix} \quad (8.13)$$

where (T_x, T_y, T_z) = thrust components

The characteristic equation of the system (12) is

$$s^2 + n^2 = 0, \quad (8.14)$$

so there is one purely oscillatory mode at frequency n . The natural motion is of the form

$$\begin{bmatrix} \delta v \\ \delta y \end{bmatrix} = c \begin{bmatrix} n \\ 0 \end{bmatrix} \cos(nt + \beta) - c \begin{bmatrix} 0 \\ -1 \end{bmatrix} \sin(nt + \beta), \quad (8.15)$$

Where c and β are arbitrary constants, and the complex eigen vector corresponding to $s = nj$ is $(n, -j)^T$. The real part of this eigen vector is the coefficient of $\cos(nt + \beta)$ while the imaginary part is the coefficient of $[-\sin(nt + \beta)]$. The motion may be interpreted as a slight change in orbit plane, so that the spacecraft crosses the reference orbital plane twice per revolution, and

thus appears to oscillate right-left with orbital frequency n . The characteristic equation of the system (13) is

$$s^2(s^2 + n^2) = 0, \quad (8.16)$$

so there is one purely oscillatory mode at frequency n , and two stationary modes. The natural motions are of the form

$$\begin{bmatrix} \delta u \\ \delta w \\ \delta x \\ \delta z \end{bmatrix} = c_1 \begin{bmatrix} 0 \\ n \\ 2 \\ 0 \end{bmatrix} \cos(nt + \beta) - c_1 \begin{bmatrix} n \\ 0 \\ 0 \\ 1 \end{bmatrix} \sin(nt + \beta) + (c_2 + c_3 nt) \begin{bmatrix} 0 \\ n \\ 1 \\ 0 \end{bmatrix} + c_3 \begin{bmatrix} n/3 \\ 0 \\ 0 \\ 2/3 \end{bmatrix}, \quad (8.17)$$

where c_1, β, c_2 , and c_3 are arbitrary constants. The first two column vectors in (17) are the real and imaginary parts of the eigenvector corresponding to $s = nj$; the third and fourth column vectors are the principal and secondary eigenvectors corresponding to $s = 0$. The motion of the perturbed spacecraft in each of these three modes, as observed from an unperturbed spacecraft in the same circular orbit, is shown in Figure 8.2.

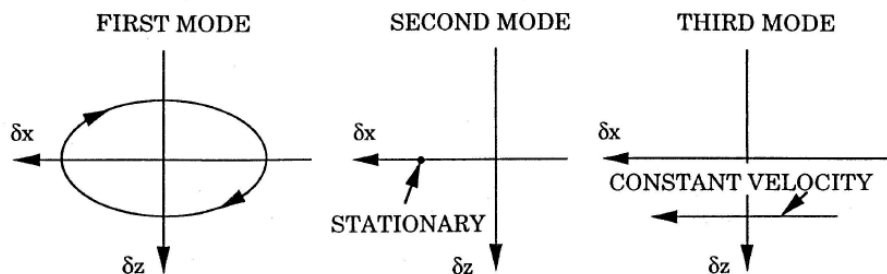


Figure 8.2 Modes of translational motion in circular orbit

The first mode ($c_1 \neq 0$) corresponds to a slightly elliptic orbit so that the spacecraft goes above the circular orbit for half a period and slows down, then goes below and speeds up for the other half. The second mode ($c_2 \neq 0$) corresponds to the spacecraft being in the same circular orbit but slightly ahead of (or behind) the reference point. The third mode ($c_3 \neq 0$) corresponds to the spacecraft being in a lower (or higher) circular orbit that has a faster (or slower) orbital velocity.[4]

In this section slow control in circular orbit; In-Track/Radial motions are considered. Equations of motion were derived in (13).

$$\begin{bmatrix} \delta\dot{u} \\ \delta\dot{w} \\ \delta\dot{x} \\ \delta\dot{z} \end{bmatrix} = \begin{bmatrix} 0 & n & -n^2 & 0 \\ -n & 0 & 0 & 2n^2 \\ 1 & 0 & 0 & n \\ 0 & 1 & -n & 0 \end{bmatrix} \begin{bmatrix} \delta u \\ \delta w \\ \delta x \\ \delta z \end{bmatrix} + \begin{bmatrix} T_x/m \\ T_z/m \\ 0 \\ 0 \end{bmatrix}$$

It is convenient to put them into dimensionless form by using the following units: time in $1/n$, ($\delta u, \delta \omega$) in nR , ($\delta x, \delta z$) in R , (T_x, T_z) in mg , where n =orbital rate(considering $n=1$), R =orbit radius (considering $R=1\text{km}$), m =mass of spacecraft(considering $m=1\text{kg}$), and g =gravitational force per unit at that orbit radius:

$$\begin{bmatrix} \delta\dot{u} \\ \delta\dot{w} \\ \delta\dot{x} \\ \delta\dot{z} \end{bmatrix} = \begin{bmatrix} 0 & 1 & -1 & 0 \\ -1 & 0 & 0 & 2 \\ 1 & 0 & 0 & 1 \\ 0 & 1 & -1 & 0 \end{bmatrix} \begin{bmatrix} \delta u \\ \delta w \\ \delta x \\ \delta z \end{bmatrix} + \begin{bmatrix} 1 & 0 \\ 0 & 1 \\ 0 & 0 \\ 0 & 0 \end{bmatrix} \begin{bmatrix} T_x \\ T_z \end{bmatrix}. \quad (8.18)$$

The transfer functions from in-track/radial thrust to in-track/radial position deviations are readily deduced from these equations:

$$\begin{bmatrix} \delta x(s) \\ \delta z(s) \end{bmatrix} = 1/s^2(s^2 + 1) \begin{bmatrix} s^2 - 3 & 2s \\ -2s & s^2 \end{bmatrix} \begin{bmatrix} T_x(s) \\ T_z(s) \end{bmatrix}. \quad (8.19)$$

There are pole-zero cancellations in three of the four transfer functions, indicating a lack of observability or controllability. Thus we shall choose δx as output (and measurement), and T_x as control, since there are no pole-zero cancellations in that transfer function.

8.3.1 Stabilization of In-Track/Radial Motions

Since all three modes are controllable with T_x , consider the LQ synthesis of a regulator using full state feedback to T_x using proportional thrusters. We take as performance index

$$J = \int_0^\infty \{A[(\delta x)^2 + (\delta z)^2] + B(T_{cx})^2\} dt. \quad (8.20)$$

It follows that the symmetric root characteristic equation (SRCE) is

$$Y^T(-s)AY(s) + B = 0, \quad (8.21)$$

where

$$\begin{bmatrix} \delta x(s) \\ \delta z(s) \end{bmatrix} = Y(s)T_{cx}(s). \quad (8.22)$$

In this case, the transfer function matrix $Y(s)$ is given by

$$Y(s) = 1/s^2(s^2+1) \begin{bmatrix} s^2 - 3 \\ -2s \end{bmatrix}. \quad (8.23)$$

Thus the SRCE is

$$[s^2-3, 2s] \begin{bmatrix} s^2 - 3 \\ -2s \end{bmatrix} + \frac{B}{A} s^4 (s^2 + 1)^2 = 0, \quad (8.24)$$

and Evans's form is given by,

$$-\frac{B}{A} = \frac{(s^2-1)(s^2-9)}{s^4(s^2+1)^2} \quad (8.25)$$

Note the "compromise" zeros at $s = \pm 1, \pm 3$. These arise from trying to control both δx and δz with only one control, T_x . Symmetric root locus (SRL) versus A/B is shown in Fig.8.3.

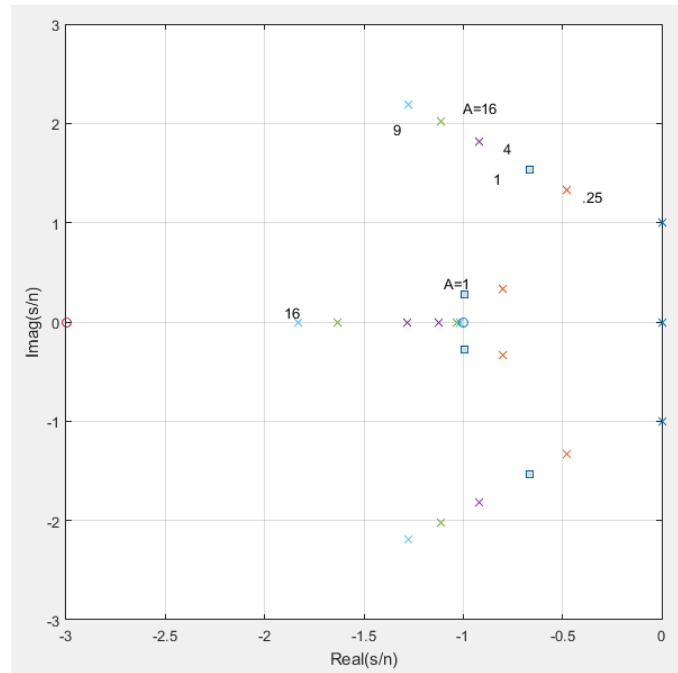


Figure 8.3 Stabilization of in-track/radial motion using proportional tangential thrusters; locus of LQ regulator poles vs A/B

For $A/B = 1$, the closed-loop regulator eigenvalues are

$$s = -0.667 \pm 1.536j, -0.996 \pm 0.279j, \quad (8.26)$$

and the corresponding state feedback is

$$T_{cx} = [-3.32, 3.27, -2.27, 5.17] \begin{bmatrix} \delta u \\ \delta w \\ \delta x \\ \delta z \end{bmatrix} \quad (8.27)$$

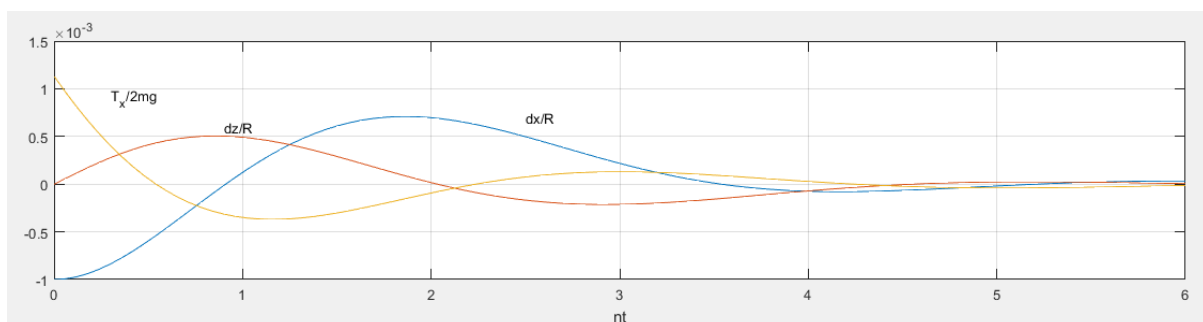


Figure 8.4 Response of controlled spacecraft to an initial in-track error $\delta x(0)/R = -0.001$ with orbital rate $n=1$

Fig. 8.4 shows the *time response*, using the control law (27), where the spacecraft is initially in circular orbit with an orbital rate $n=1$, but has an in-track error (blue), $\delta x(0)/R = -.001$, $\delta z(0) = 0$, $\delta u(0) = 0$, $\delta w(0) = 0$. The error is eliminated in roughly one orbital period ($nt = 2n$); the in-track error overshoots by 70% and returns to zero; the radial displacement (yellow) is first down ($\delta z > 0$) and then up; the thrust is positive to start with $2.265 \times 10^{-3} \times mg$, and it alternates sign about three times in the first orbit.

Similarly for orbital rate $n=2$

For $A/B = 1$,

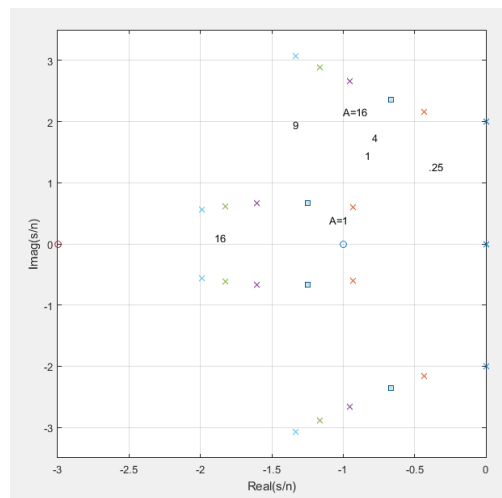


Figure 8.5 Stabilization of in-track/radial motion using proportional tangential thrusters; locus of LQ regulator poles vs A/B

the closed-loop regulator eigenvalues are

$$s = -.6629 \pm 2.359j, -1.25 \pm .66j, \quad (8.28)$$

and its corresponding control law is

$$T_{cx} = [3.8249, -2.0787, 3.154, 8.237] \begin{bmatrix} \delta u \\ \delta w \\ \delta x \\ \delta z \end{bmatrix} \quad (8.29)$$

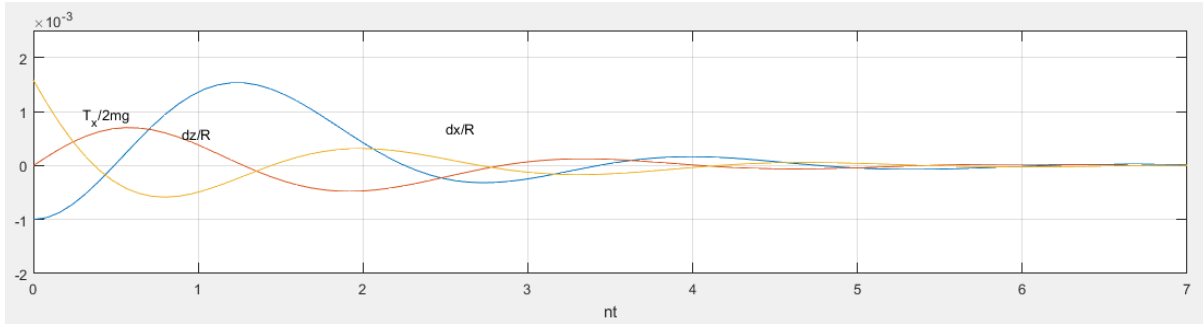


Figure 8.6 Response of controlled spacecraft to an initial in-track error $\delta x(0)/R = -.001$ with orbital rate $n=2$

Similarly, Fig. 8.6 shows the *time response*, for orbital rate $n=2$, where the spacecraft is initially in circular orbit but has an in-track error. The error is eliminated in four orbital period ($nt = 2n$); the in-track error overshoots by 85% and returns to zero; the radial displacement is first down ($\delta z > 0$) and then up; the thrust is positive to start with $2.565 \times 10^{-3} \times mg$, and it changes sign about six times in the first orbit.

Comparing figure 8.4 and figure 8.6 denotes that with increase in orbit rate the in-track error takes more time to return to zero. Hence, increase in orbital rate may cause more delay in settling of in-track errors.

Conclusion and further works

In section 3, Attitude control of satellite having reaction wheel using Bang-Off-Bang control is done. When the external disturbance is given, it causes θ and $\dot{\theta}$ values to vary. This fluctuation has been controlled by implementation of the PI feedback controller and thruster as an actuator. Finally the variation caused by the external disturbance is reduced and the θ , $\dot{\theta}$ values returns to nearly to zero. θ and $\dot{\theta}$ takes almost 10 seconds to settle. Further work will be reducing the settling time of the system by using other control techniques.

In section 4, Attitude control with reaction wheel is discussed. Coupling action of yaw and roll are considered. Slow Roll/Yaw control using gravity desaturation is analysed. State feedback control law is obtained and validated in the closed loop response. Also the response of the closed loop system to an impulsive roll and yaw disturbance for the slow roll/yaw control using roll and yaw reaction wheels and gravity desaturation is discussed. Also found ϕ and ψ reaches its peak value and then it follows the desaturation period. As the gravity torque acts only in roll, the roll coupling is large when compared with the yaw coupling is also found. In this thesis only 2 axis control is discussed. Further work will be considering 3 axis satellite control involving Pitch, Yaw and Roll.

In section 5, Spin stabilization scenarios are discussed. It is also found that the satellite will be stable only if it is spinning in major axis. It becomes as a constrain of not using satellite in its minor axis. Further work will considering the dual spin conditions, which allows the satellite to use in minor axis.

In section 6, Attitude control with gimballed momentum wheel is considered. Both passive and active control has been analysed. Normalized value of K has been obtained. Only in active control the ϕ and ψ are returned to zero by over-transferring the angular momentum to the GMW from spacecraft, then using the excess to bring S/C attitude to zero. The analysis is done only for two gimbal momentum wheels. Further, it can be extended for three gimbal momentum wheels and their coupling effects has to be analysed.

In section 7, Attitude control schemes during thrust maneuvers using gimballed engine is analysed. Control law is obtained for the chosen weighting factor, A. Also the closed loop response for a initial pitch rate is obtained.

In section 8, State feedback control law is obtained for the considered weighting factor and the response of the controlled spacecraft to an in-track error is analysed

Most of the satellite parameters used in the thesis are thought-out values. Further work should include the existing satellite mission parameters.

References

- [1]- <http://goes.gsfc.nasa.gov/text/databook/section11.pdf>, 2016 ,25th June 2016.
- [2]- James R. Wertz. Spacecraft Attitude determination and Control. Astrophysics and Space Science Library, 2002.
- [3] Jack B. Kuipers. Quaternions & Rotation Sequences - A Primer with Applications to Orbits, Aerospace, and Virtual Reality. 1999.
- [4] Arthur E. Bryson ,Jr , Control of spacecraft and aircraft,1994 by Princiton university Press Publication
- [5] W. H. Steyn, “A view finder control system for an earth observation satellite,” Aerospace Science and Technology, vol. 10, n. 3, pp. 248- 255, April, 2006.
- [6] R. Kristiansen, O. Egeland and P. Johan, “A comparative study of actuator configurations for satellite attitude control,” Modelling, Identification and Control, vol. 26, n. 4, pp. 201-219, Dec 2005.
- [7] S. Y. Yong, “Development of reaction wheels housing for microsatellites,” Aircraft Engineering and Aerospace Technology, vol. 77, n. 2, pp. 114-121, 2005.
- [8] G. Shengmin and C. Hao, “A comparative design of satellite attitude control system with reaction wheel,” in Proceedings of First NASA/ESA Conference on Adaptive Hardware and Systems, pp. 359- 362, 2006.
- [9] https://en.wikipedia.org/wiki/Reaction_wheel,2017 ,24th April
- [10] Esaú Vicente-Vivas , Emilio Jiménez , Rodrigo Alva,Rodrigo Córdova,“Attitude Subsystem Development for an Educative Satellite Based on Reaction/Momentum Wheel and Magnetic Torquing Coils” Research On Computer Science, Special Issue: Industrial Informatics, Vol. 31, pp.133-142 , ISSN: 1870-4069, Centro de Investigación en Computación, IPN, México, DF, November 2007. Indexed in LATINDEX.
- [11]-"R Votel, D Sinclair. "Comparison of control moment gyros and reaction wheels for small Earth-observing satellites." 26th Annual AIAA/USU Conference on Small Satellites.
- [12]-<http://www.sciencedirect.com/science/article/pii/S0094576584900365>,24th April 2017.

[13]-<https://geekswipe.net/technology/aerospace/how-reaction-wheels-and-control-moment-gyros-work/>.,24th April 2017

[14]-<http://blog.vibratechtd.com/blog/how-does-a-viscous-damper-work>. 24th April 2017

[15]- Nishihara Osamu,Matsuhisa Hiroshi,Sato Susumu.Transactions of the Japan Society of Mechanical Engineers Series A 59(560), 1053-1061, 1993

[16] Spacecraft attitude control during thrusting maneuvers - Space vehicle design criteria /Guidance and control. NASA-SP-8059.

[17] <https://spaceflight systems.grc.nasa.gov/education/rocket/gimbaled.html> ,24th April,2017

[18]Lunar Orbiter Design Survey Team: Lunar Orbiter Program-Guidance and Control System Design Survey. The Boeing Company Document No. D2-114277-3, May 9, 1969.

Appendix:

Matlab code:

Chapter 4

```
% % Figure 4.2 Locus of closed-loop poles vs A for slow roll/yaw control
using roll and yaw reaction wheels and gravity desaturation; a=b=.5;
n=pi/50; epX=epz=.025;x=[phi p Hx psi r Hz]'; u=[ex ez]';

a=.5;
b=.5;
n=pi/50;
epX=.025;
epz=.025;
F=[0 1 0 n 0 0;-3*a*n^2 -1 1/(1+epX) 0 -a*n 0
    -3*a*n^2 0 0 0 -a*n 0;
    -n 0 0 0 1 0;
    0 b*n 0 0 -1 1/(1+epz);
    0 b*n 0 0 0 0];
G=[0 1 0 0 0 0; 0 0 0 0 1 0]';
H=[1 0 0 0 0 0;0 0 0 1 0 0];
A1=eye(2); B=eye(2);
A=[0:.002:.02]'; ev=zeros(6,11);
for i=1:11,
    k=lqr(F,G,A(i)*H'*A1*H,B);
    ev(:,i)=eig(F-G*k);
end
%
figure(1); clf;
subplot(121),
plot(real(ev),imag(ev),'x',-.004,.004,'o');
```

```

grid; axis([-1 -.9 -.02 .02]); axis('square')
xlabel('Real(s/\sigma)'); ylabel('Imag(s/\sigma)')
text(-.99,.01,'Reaction Wheels'); text(-.965,.07,'dA=.002')
text(-.985,.05,'n=(\pi/50)*\sigma');

subplot(122), plot(real(ev),imag(ev),'x');
grid; axis([-1 0 -1 .1]);
axis square
xlabel('Real(s/\sigma)'); text(-.025,.078,'Roll')
text(-.025,.045,'Yaw'); text(-.075,.0825,'A=.01')
text(-.06,.01,'.01'); text(-.03,.01,'.01'); text(-.012,.01,'TZ')

```

```

%Figure 4.3 Response to an impulsive roll disturbance for slow roll/yaw
&control using roll and yaw reaction wheels and gravity desaturation
%stabilization of oblate S/C w. symmetry axis cross-track & response to
%impulsive roll disturbance torque;
% s=[phi p Hx psi r Hz]'; u=[ex ez]'; time in units of 1/n,
% (p r Hx/Ix Hz/Iz sg) in n, u in R*I*n^2/N;
%
tf=2*pi; Ns=100; a=.5; b=.5; sg=50/pi; ep=.025;
A=[0 1 0 1 0 0;
   -3*a -sg sg*(1-ep) 0 -a 0;
   -3*a 0 0 0 -a 0;
   -1 0 0 0 1 0;
   0 b 0 0 -sg sg*(1-ep);
   0 b 0 0 0 0];
B=[0 1 0 0 0 0; 0 0 0 0 1 0]';
C=[1 0 0 0 0 0; 0 0 0 1 0 0];
s0=[0 1 1 0 0 0]';
Q=1000*eye(2); R=eye(2);

```



```

k=lqr(A,B,C'*Q*C,R); C1=[eye(6); 0 -1 1 0 0 0; 0 0 0 0 -1 1; -k];
D1=zeros(10,2); t=2*pi*[0:.01:1]';

u=zeros(101,2); y=lsim(A-B*k,B,C1,D1,u,t,s0); t=t/(2*pi);

%
figure(1); clf; subplot(221), plot(t,y(:,[1:3])); grid;
axis([0 1 -.2 1]); legend('\phi','p','H_x');
subplot(222), plot(t,y(:,[4:6])); grid; axis([0 1 -.2 1]);
legend('\psi','r','H_z');
subplot(223), plot(t,y(:,7),t,-y(:,9)/10); grid;
axis([0 1 -.2 1]); xlabel('nt/2\pi');
legend('e_x','-epsilon*p_w/10');
subplot(224), plot(t,y(:,8),t,-y(:,10)/10); grid;
axis([0 1 -1 .2]); xlabel('nt/2\pi');
legend('e_z','-epsilon*r_w/10',4);

% Figure 4.4 Response to an impulsive roll disturbance for slow roll/yaw
control using roll and yaw reaction wheels and gravity desaturation
s=[phi p Hx psi r Hz]'; u=[ex ez]'; time in units of 1/n, (p r Hx/Ix
Hz/Iz sg)% in n, u in R*I*n^2/N;

tf=2*pi;
Ns=100;
a=.5;
b=.5;
sg=50/pi;
ep=.02;
A=[0 1 0 1 0 0;
   -3*a -sg sg*(1-ep) 0 -a 0;
   -3*a 0 0 0 -a 0;
   -1 0 0 0 1 0;
   0 b 0 0 -sg sg*(1-ep);
   0 b 0 0 0 0];

```

```

B=[0 1 0 0 0 0; 0 0 0 0 1 0]';
C=[1 0 0 0 0 0; 0 0 0 1 0 0];
s0=[0 0 0 0 1 1]';
Q=1000*eye(2); R=eye(2);
k=lqr(A,B,C'*Q*C,R);
C1=[eye(6); 0 -1 1 0 0 0; 0 0 0 0 -1 1; -k]; D1=zeros(10,2);
t=2*pi*[0:.01:1]'; u=zeros(101,2);
y=lsim(A-B*k,B,C1,D1,u,t,s0); t=t/(2*pi);
%
figure(1); clf; subplot(221), plot(t,y(:,[1:3])); grid;
legend('\phi','p','H_x'); axis([0 1 -.5 1]);
subplot(222), plot(t,y(:,[4:6])); grid;
legend('\psi','r','H_z'); axis([0 1 -.5 1]);
subplot(223), plot(t,y(:,7),t,-y(:,9)/10); grid;
xlabel('nt/2\pi'); axis([0 1 -.5 1]);

legend('e_x','- \epsilon p_w/10');
subplot(224),plot(t,y(:,8),t,-y(:,10)/10); grid;
xlabel('nt/2\pi'); axis([0 1 0 1.5]);
legend('e_z','- \epsilon r_w/10');

```

Chapter 5

```

%%Figure 5.3 Root locus vs damping constant D for disk-like spacecraft
with nutation damping wheel x=[p,r,Om]'; la=Is/IT; ep=Iw/IT; % time in
1/ws, x in ws=spin rate;
% D in units of Iw*ws;

ep=.06;
la=1.8;

```

```
J=[1 0 0;0 1 ep;0 1 1];
C=[0 la-1 -ep;-(la-1) 0 0;0 0 0];
C1=zeros(3);C1(3,3)=-1;
D=[0:1/6:1]'; ev=zeros(3,7);
for i=1:7, ev(:,i)=eig(J\(C+D(i)*C1));
end
%
figure(1); clf; subplot(121),plot(real(ev),imag(ev),'x',0,.5,'o');
grid; axis([-1 .1 -1 1]);axis('square'); xlabel('Real(s/\omega_s)');
ylabel('Imag(s/\omega_s)'); text(-.35,.425,'Nutation');
text(-.475,.025,'D=.5'); subplot(122),
plot(real(ev),imag(ev),'x',0,.5,'o'); grid; axis([-0.04 .04 .4 .9]);
axis square; xlabel('Real(s/\omega_s)'); text(-.005,.491,'D=.5');
```

```
% Figure 5.4. Response of disk-like spacecraft with nutation damping
wheel to an impulsive roll disturbance torque % x=[p,r,Om]'; la=Is/IT;
ep=Iw/IT; time in 1/ws, D in Iw*ws;
```

```
ep=.06;
la=1.8;
D=.5;
J=[1 0 0; 0 1 ep;0 1 1]; C=[0 la-1 -ep; -(la-1) 0 0; 0 0 -D];
F=J\C;G=[1 0 0]'; H=eye(3);
L=zeros(3,1);
x0=[1 0 0]'; t=(2*pi)*[0:.02:20]'; u=zeros(1001,1);
y=lsim(F,G,H,L,u,t,x0);
%
figure(1); clf; subplot(211), plot(t/(2*pi),y(:,1)); axis([0 20 -4 4])
grid; ylabel('p/\omega_s'); subplot(212), plot(t/(2*pi),y(:,3));
axis([0 20 -2 2]) ; grid; xlabel('\omega_s t/(2\pi)')
```

```
ylabel('\omega/\omega_s')
```

```
%Figure 5.5 Root locus vs damping constant D for rod-like spacecraft with
nutration damping wheel. x=[p,r,om]'; la=Is/IT; ep=Iw/IT; time in 1/ws, x
in ws=spin rate;
```

```
ep=.06;
la=.8;
J=[1 0 0;0 1 ep;0 1 1];
C=[0 la-1 -ep;-(la-1) 0 0;0 0 0];
C1=zeros(3);C1(3,3)=-1;
D=[0:1/6:1]'; ev=zeros(3,7);
for i=1:7, ev(:,i)=eig(J\(C+D(i)*C1));
end
%
figure(1); clf; subplot(121),plot(real(ev),imag(ev),'x',0,.5,'o');
grid; axis([-1 .1 -1 1]);axis('square'); xlabel('Real(s/\omega_s)');
ylabel('Imag(s/\omega_s)'); text(-.35,.425,'Nutration');
text(-.475,.025,'D=.5'); subplot(122),
plot(real(ev),imag(ev),'x',0,.5,'o'); grid; axis([-0.04 .04 -.5 .7]);
axis square; xlabel('Real(s/\omega_s)'); text(-.005,.491,'D=.5');
```

```
%Figure 5.6. Response of rod-like spacecraft with nutration damping wheel
to an impulsive roll disturbance torque . x=[p,r,Om]'; la=Is/IT;
ep=Iw/IT;time in 1/ws;
```

```

ep=.06;
la=.8;
D=.5;
J=[1 0 0; 0 1 ep;0 1 1];
C=[0 la-1 -ep; -(la-1) 0 0; 0 0 -D]; F=J\C;G=[1 0 0]'; H=eye(3);
L=zeros(3,1);
x0=[1 0 0]'; t=(2*pi)*[0:.02:20]'; u=zeros(1001,1);
y=lsim(F,G,H,L,u,t,x0);
%
figure(1); clf; subplot(211), plot(t/(2*pi),y(:,1)); axis([0 20 -4 4])
grid; ylabel('p/\omega_s'); subplot(212), plot(t/(2*pi),y(:,3));
axis([0 20 -2 2]) ; grid; xlabel('\omega_s t/(2\pi)')
ylabel('\omega/\omega_s')

```

Chapter 6

```

% Figure 6.5. Response of S/C with a GMW with passive control of GMW to
impulsive roll and yaw disturbance torques with viscous damper between
S/C and outer gimbal.(phi,psi) sensors and gimbal torque actuators; RL
vs. K; xdot=Fx+Ga*w; x=[phig,psig,phi,% psi]'; w=[Hx,Hz]'; t in units of
Ix/h, (Hx,Hz,D) in units of h; Iz in % units of Ix; K in units of h^2/Ix;

D=1;
Iz=1;
F=[-D/Iz -D^2 0 0;
    D^2/Iz -D 0 0]/(1+D^2);
F=[F; 0 -1 0 0; 1/Iz 0 0 0];
Ga=[D^2 -D/Iz; D D^2/Iz]/(1+D^2);
Ga=[Ga; 1 0; 0 1/Iz];
H=eye(4); L=zeros(4,2); t=[0:.06:6]';
yr=step(F,Ga,H,L,1,t);

```

```

%
figure(1); clf; subplot(211), plot(t,yr); axis([ 0 6 0 1.5]); grid
xlabel('t*h/Ix'); text(1.3,1.1, '\phi'); text(3.7,.25, '\phi_g')
text(3.2,.6, '\psi'); text(1.3,.75, '\psi_g'); yy=step(F,Ga,H,L,2,t);
subplot(212), plot(t,yy); grid; axis([0 6 -1.5 1.5])
xlabel('t*h/I_x');text(1.5,.6, '\psi'); text(2.5,.5, '\psi_g')
text(2.5,-.5, '\phi'); text(.5,-.85, '\phi_g')

%%Figure 6.6 Locus of closed-loop poles vs K for active control of S/C
with a GMW. (phi,psi) sensors and gimbal torque actuators; RL vs. K;
xdot=Fx+Ga*w; x=[phig,psig,phi,psi]'; w=[Hx,Hz]'; t in units of Ix/h,
(Hx,Hz,D) in units of h; Iz in units of Ix; K in units of h^2/Ix;

D=1;
Iz=1.2;
K=[0:.05:.8]';
ev=zeros(4,5);
for i=1:17
    F=[-D/Iz -D^2 K(i)*D -K(i);
        D^2/Iz -D K(i) K(i)*D]/(1+D^2);
    F=[F; 0 -1 0 0; 1/Iz 0 0 0];
    ev(:,i)=eig(F);
end
%
figure(1); clf; plot(real(ev),imag(ev), 'x'); axis([-1 0 -1 1])
axis('square'); grid; xlabel('Real(s*I_x/h)'); ylabel('Imag(s*I_x/h)')
text(-.3,.5, 'K=.25'); text(-.18,.9, '.75'); text(-.3,.8, 'Roll')
text(-.22,.75, '.5'); text(-.46,.55, '.125'); text(-.2,.2, 'Yaw')

```

```

%%Figure 6.7 Response of S/C with active control of a GMW to impulsive
roll and yaw disturbance torques. (phi,psi) sensors
% and gimbal torque actuators; xdot=Fx+Ga*w; x=[phig,psig,phi,psi]';
% w=[Hx,Hz]'; t in units of Ix/h, (Hx,Hz,D) in units of h; Iz in units
% of Ix; K in units of h^2/Ix;

D=1;
Iz=1;
K=.25;
F=[-D/Iz -D^2 K*D -K; D^2/Iz -D K K*D]/(1+D^2);
F=[F; 0 -1 0 0; 1/Iz 0 0 0];
Ga=[D^2 -D/Iz; D D^2/Iz]/(1+D^2);
Ga=[Ga;1 0;0 1/Iz]; H=eye(4); L=zeros(4,2); t=[0:.16:16]';
yr=step(F,Ga,H,L,1,t);
%
figure(1); clf;

subplot(211), plot(t,yr); grid; axis([0 16 -.5 1.5])
xlabel('t*h/I_x'); text(.6,1,'\phi'); text(2.2,-.3,'\phi_g')
text(6,.7,'\psi'); text(6,1.2,'\psi_g')
yy=step(F,Ga,H,L,2,t);

subplot(212), plot(t,yy); grid
axis([0 16 -1.5 1.5]); xlabel('t*h/I_x'); text(5,.5,'\psi')
text(2,.5,'\psi_g'); text(2.5,-.45,'\phi'); text(.6,-1.3,'\phi_g')

```

Chapter 7

```

% % Figure 7.4 Spacecraft with gimbaleed engine;locus of LQ regulator
poles vs weighting factor A
% x=[om ome del the]; u=Q; xdot=Ax+Bu; y=Qx;
ep=.11851;

```

```

la=100.78;
A=[0 0 -ep 0; 0 0 1-ep 0; -1 1 0 0; 1 0 0 0];
B=[1 -la 0 0]';
C=[0 0 0 1];
A1=[.001 .003 .01 .03 .1 .3 1]';
ev=zeros(4,8);
ev(:,1)=eig(A);

for i=1:7,
    k=lqr(A,B,C'*A1(i)*C,1);
    ev(:,i+1)=eig(A-B*k);
end
%
figure(1); clf; plot(real(ev),imag(ev),'x'); axis([-2 0 -2 2])
axis('square'); grid; xlabel('Real(s/p)'); ylabel('Imag(s/p)')
text(-1.8,.75,'A=1'); text(-1.55,.59,'.3'); text(-1.4,.46,'.1')
text(-1.2,.35,'.03'); text(-1.1,.27,'.01'); text(-.95,.19,'.003')
text(-.92,.1,'.001'); text(-.9,1.49,'A=1'); text(-.7,1.05,'.1')
text(-.65,.7,'.01'); text(-.6,.41,'.001')

```

```

% Figure 7.5 Spacecraft with gimbaled engine; response to initial angular
velocity  $\omega(0)=p$ ;  $x=[\omega, \omega_e, \delta, \theta]$ ;

```

```

%  $u=Q$ ;  $\dot{x}=Fx+Gu$ ;  $y=Hx$ ;

```

```

ep=.11851;
la=100.78;
F=[0 0 -ep 0;
    0 0 1-ep 0;
    -1 1 0 0;
    1 0 0 0];

```



```
G=[1 -1a 0 0]';
H=[0 0 0 1];
K=lqr(F,G,H'*.01*H,1);
x0=[1 0 0 0]';
t=[0:.14:14]';
u=zeros(1,101); H1=[eye(4); -k]; L1=zeros(5,1);
y=lsim(F-G*K,G,H1,L1,u,t,x0);
%
figure(1); clf; subplot(211), plot(t,y(:,3),t,5*y(:,4),t,2*y(:,5));
axis([0 14 -5 10]); grid; xlabel('pt'); text(3.5,6,'5*\theta')
text(6,-3.6,'\delta'); text(1,-4,'2*Q/b')
```

Chapter 8

```
% Figure 8.3 Stabilization of in-track/radial motion using proportional
tangential thrusters; locus of LQ regulator poles vs A/B;
x=[du,dw,dx,dz]'; u=Tx; y=[dx,dz]'; time in 1/n, (du,dw) in nR, (dx,dz) in
R, Tx in mg, R=earth radius,% n=orbit rate;
```

```
A=[0 1 -1 0;
    -1 0 0 2;
    1 0 0 1;
    0 1 -1 0];
B=[1 0 0 0]';
C=[0 0 1 0;0 0 0 1];
Q=[.25 1 4 9 16]';
ev=zeros(4,6); ev(:,1)=eig(A);
for i=1:5,k=lqr(A,B,C'*Q(i)*C,1); ev(:,i+1)=eig(A-B*k); end
%
figure(1); clf; plot(real(ev),imag(ev),'x',-3,0,'o',-1,0,'o');
```

```
axis([-3 0 -3 3]); axis('square'); grid; xlabel('Real (s/n)')
ylabel('Imag (s/n)'); text(-1,2.16,'A=16'); text(-1.35,1.95,'9')
text(-.8,1.75,'4'); text(-.85,1.45,'1'); text(-.4,1.27,'.25')
text(-1.1,.4,'A=1'); text(-1.9,.1,'16')
```

```
% Figure 8.4 Response of controlled spacecraft to an initial in-track
error  $x(0)/R = -.001$  with orbital rate  $n=1$ ;  $x=[du,dw,dx,dz]'$ ;  $u=Tx$ ;
 $y=[dx,dz]'$ ; time in  $1/n$ ,  $(du,dw)$  in  $nR$ ,  $(dx,dz)$  in  $R$ ,  $Tx$  in  $mg$ ,  $R=earth$ 
radius,  $n=orbit$  rate;
```

```
F=[0 1 -1 0;
    -10 0 0 2;
    1 0 0 1;
    0 1 -1 0];
G=[1 0 0 0]';
L=[0 0]';
H=[0 0 1 0; 0 0 0 1];
k=lqr(F,G,H'*H,1);
t=[0:.08:8]'; u=zeros(101,1);
x0=[0 0 -.001 0]';
H1=[H; -k]; L1=[L;0];
y=lsim(F-G*k,G,H1,L1,u,t,x0);
%
figure(1); clf; subplot(211), plot(t,y(:,1:2),t,y(:,3)/2); grid
axis([0 7 -.002 .0025]); xlabel('nt'); text(.3,.0009,'T_x/2mg')
text(.9,.0006,'dz/R'); text(2.5,.0007,'dx/R')
```

```
% Figure 8.5 Stabilization of in-track/radial motion using proportional
tangential thrusters; locus of LQ regulator poles vs A/B;
 $x=[du,dw,dx,dz]'$ ;  $u=Tx$ ;  $y=[dx,dz]'$ ; time in  $1/n$ ,  $(du,dw)$  in  $nR$ ,  $(dx,dz)$  in
 $R$ ,  $Tx$  in  $mg$ ,  $R=earth$  radius, %  $n=orbit$  rate,  $n=2$ ;
```

```
A =[0 2 -4 0;
```

```

-2 0 0 8;
1 0 0 2;
0 1 -2 0];
B=[1 0 0 0]';
C=[0 0 1 0;0 0 0 1];
Q=[.25 1 4 9 16]'; ev=zeros(4,6); ev(:,1)=eig(A);
for i=1:5,k=lqr(A,B,C'*Q(i)*C,1); ev(:,i+1)=eig(A-B*k); end
%
figure(1); clf; plot(real(ev),imag(ev),'x',-3,0,'o',-1,0,'o');
axis([-3 0 -3.5 3.5]); axis('square'); grid; xlabel('Real(s/n)')
ylabel('Imag(s/n)'); text(-1,2.16,'A=16'); text(-1.35,1.95,'9')
text(-.8,1.75,'4'); text(-.85,1.45,'1'); text(-.4,1.27,'.25')
text(-1.1,.4,'A=1'); text(-1.9,.1,'16')

```